

## Divergent shifts in peak photosynthesis timing of temperate and alpine grasslands in China

Jilin Yang<sup>a,b</sup>, Jinwei Dong<sup>a,\*</sup>, Xiangming Xiao<sup>c</sup>, Junhu Dai<sup>a</sup>, Chaoyang Wu<sup>a</sup>, Jianyang Xia<sup>d</sup>, Guosong Zhao<sup>a</sup>, Miaomiao Zhao<sup>e,b</sup>, Zhaolei Li<sup>f</sup>, Yao Zhang<sup>g</sup>, Quansheng Ge<sup>a,\*</sup>

<sup>a</sup> Key Laboratory of Land Surface Pattern and Simulation, Institute of Geographic Sciences and Natural Resources Research, Chinese Academy of Sciences, Beijing 100101, China

<sup>b</sup> University of Chinese Academy of Sciences, Beijing 100049, China

<sup>c</sup> Department of Microbiology and Plant Biology, Center for Spatial Analysis, University of Oklahoma, Norman, OK 73019, USA

<sup>d</sup> Tiantong National Station of Forest Ecosystem and Research Center for Global Change and Ecological Forecasting, School of Ecological and Environmental Sciences, East China Normal University, Shanghai 200241, China

<sup>e</sup> State Key Laboratory of Resources and Environmental Information System, Institute of Geographic Sciences and Natural Resources Research, Chinese Academy of Sciences, Beijing 100101, China

<sup>f</sup> Key Laboratory of Ecosystem Network Observation and Modeling, Institute of Geographic Sciences and Natural Resources Research, Chinese Academy of Sciences, Beijing 100101, China

<sup>g</sup> Department of Earth and Environmental Engineering, Columbia University, New York, NY 10027, USA

### ARTICLE INFO

#### Keywords:

Peak photosynthesis timing  
Grassland peak phenology  
Photosynthetic seasonality  
Gross primary production  
Interannual variation

### ABSTRACT

The changing climate is shifting the seasonality of photosynthesis in vegetation, including the start (SOS), end (EOS), and length (LOS) of the growing season, and the peak photosynthesis timing (PPT). While the SOS, EOS, and LOS have been widely investigated, the PPT of grasslands – as a proxy for the response of seasonal plant photosynthesis to climate change – has been overlooked. In this study, we propose a hybrid generalized additive model (HGAM) method to extract PPT using the Vegetation Photosynthesis Model (VPM)-based gross primary production (GPP) product, and we examine the dynamics, drivers, and consequences of PPT changes in temperate and alpine grasslands in China over 2000–2016. We found that the PPTs in temperate and alpine grasslands have exhibited advancing (with  $-0.68$  days  $\text{yr}^{-1}$ ,  $p < 0.05$ ) and delaying (with  $0.29$  days  $\text{yr}^{-1}$ ,  $p = 0.158$ ) trends, respectively. In addition, pre-season precipitation and soil moisture were positively correlated with the PPT in temperate and alpine grasslands, respectively, while the pre-season temperature consistently controlled the PPT changes in both grasslands. Furthermore, we found that an earlier PPT was associated with higher annual production in the temperate grasslands but not in the alpine grasslands in China. The divergent PPT patterns indicated the varied adaptation characteristics to climatic constraints in the temperate and alpine grasslands and also caused different consequences on carbon uptake. This study highlights the importance of PPT in understanding the spatiotemporal dynamics of vegetation photosynthesis and the carbon cycle under a changing climate.

### 1. Introduction

Understanding the mechanism driving interannual variations in annual gross primary production ( $\text{GPP}_{\text{annual}}$ ) is critical for more accurately predicting the responses of the carbon cycle to future climate change (Anav et al., 2015; Poulter et al., 2014). Previous efforts found that the variance in  $\text{GPP}_{\text{annual}}$  is mainly controlled by the length of the growing season and the maximum photosynthetic production ( $\text{GPP}_{\text{max}}$ ) (Liu et al., 2018; Xia et al., 2015; Zhou et al., 2017). Specifically,

advances in the start of the growing season (SOS) and delays in the end of the growing season (EOS) have extended the growing season or photosynthetic active period and have consequently enhanced the annual vegetation production in northern ecosystems, such as North American grasslands (Hufkens et al., 2016; Xu et al., 2016). While the dynamics of land surface phenology, especially the SOS and EOS, have been well studied (Garonna et al., 2014; Keenan et al., 2014; Piao et al., 2017; Richardson et al., 2010), the dynamics of  $\text{GPP}_{\text{max}}$ , especially the timing of  $\text{GPP}_{\text{max}}$  (namely, the peak photosynthesis timing (PPT)), have

\* Corresponding authors at: Institute of Geographic Sciences and Natural Resources Research, Chinese Academy of Sciences, 11A, Datun Road, Chaoyang District, Beijing 100101, China.

E-mail addresses: [dongjw@igsrr.ac.cn](mailto:dongjw@igsrr.ac.cn) (J. Dong), [geqs@igsrr.ac.cn](mailto:geqs@igsrr.ac.cn) (Q. Ge).

<https://doi.org/10.1016/j.rse.2019.111395>

Received 8 January 2019; Received in revised form 11 August 2019; Accepted 22 August 2019

Available online 31 August 2019

0034-4257/ © 2019 Elsevier Inc. All rights reserved.

been relatively little studied in the field (Gonsamo et al., 2018), especially for grasslands with clear seasonality. The PPT of grasslands corresponds to the timing of maximum resource availability, which affects the habitat and forage for livestock (Xu et al., 2016). A shift in PPT is considered to be an ecophysiological adaptation of plants to changes in the environment to reduce the costs for optimal growth (Schimel, 2010; Xu et al., 2016) and is expected to disrupt the synchrony of biotic interactions via mismatches in the plant-pollinator biorhythm (Hegland et al., 2009).

Previous studies on the PPT have generally been based on long-term satellite-derived Normalized Difference Vegetation Index (NDVI) datasets (mostly the biweekly 8 km GIMMS NDVI3g product; <http://ecocast.arc.nasa.gov/>) and parameter-based double logistic function (DLF) fitting methods (Gonsamo et al., 2018; Xu et al., 2016). A variety of forms of DLF methods have been developed and widely used to estimate phenological indices of vegetation (e.g., SOS and EOS) and to examine their dynamics in response to climate change at the site scale, regional scale and larger scales (Beck et al., 2006; Elmore et al., 2012; Gonsamo et al., 2018; Gu et al., 2009). To our limited knowledge, the PPT retrieval and trend analyses at the landscape level can be improved in two ways: input data and method. In terms of input data, previous studies indicated that the NDVI-derived phenological metrics cannot be used as a surrogate for phenology of canopy photosynthesis and its seasonal changes in many boreal and temperate vegetation ecosystems (Shen et al., 2014a) because NDVI can better reflect ecosystem structure (e.g., leaf area index (LAI) and aboveground green biomass) rather than ecosystem function (e.g., chlorophyll content and biological activity) (Shen et al., 2015a; Wu et al., 2017). GPP provides more detailed information on the PPT of grasslands than does NDVI. Several global GPP products with a high temporal resolution and spatial continuity (8-day, 500 m~1 km) are now available, for example, the Vegetation Photosynthesis Model (VPM) GPP (Zhang et al., 2017) and Breathing Earth System Simulator (BESS) GPP products (Jiang and Ryu, 2016; Ryu et al., 2011). The VPM GPP product has been evaluated and shown to be reliable in previous studies (Dong et al., 2015; Wagle et al., 2014; Zhang et al., 2017). In terms of PPT retrieval methods, the traditional parameter fitting methods (e.g., the DLF and asymmetric Gaussian function) are not sensitive to fluctuations (e.g., declining greenness or GPP) in the vegetation growth trajectory in the maturity phase (Elmore et al., 2012). The shape of the fitted NDVI curve generally shows a plateau during the peak season and tends to mask the actual changes in vegetation growth during this period due to disturbances such as drought (Huete et al., 2006). Therefore, a previous study assumed that the peak of photosynthesis occurs at the midpoint between the start and end of the peak season on the growth curve (Gonsamo et al., 2018). However, it is unclear if this method works well when using GPP as the input. Potential improvements in the estimation of the PPT of grasslands in this study include 1) the replacement of NDVI with GPP as the input data to better characterize the seasonal dynamics of photosynthesis and 2) the use of a more suitable fitting method for PPT estimates.

Previous studies have reported the springward shifts in PPT in the northern hemisphere using remote sensing-based observations (Gonsamo et al., 2018; Park et al., 2019; Xu et al., 2016). The interannual variation in GPP and PPT is controlled by multiple climatic factors (e.g., temperature, water availability, radiation, etc.) (Park et al., 2019). Previous studies have mostly analyzed the relationship between PPT and individual climatic factors, such as temperature or precipitation (Gonsamo et al., 2018; Xu et al., 2016; Zhou and Jia, 2016; Zu et al., 2018), and found that temperature is the main driver of the seasonal shifts in photosynthesis (Xu et al., 2016). Increased water availability due to thawing of permafrost has resulted in a stronger greening trend in boreal forests of Siberia than in North America (Forkel et al., 2015), revealing that water availability was also a co-dominant control on the seasonal dynamics and interannual changes and trends of photosynthesis (Forkel et al., 2015; Park et al., 2019).

Many studies have also shown that considerable spatial differences exist in the primary influencing factors (Forkel et al., 2015; Misra et al., 2018). However, the geographically variable relationships between vegetation PPT and multiple climatic factors (temperature, precipitation, solar radiation, and soil moisture) at the regional scale remain poorly understood. The temperate grasslands and alpine grasslands in China have different mechanisms in the carbon and water cycles (Ge et al., 2018). The seasonal photosynthetic responses of the temperate and alpine grasslands in China to climate change show different patterns according to model simulations (Liu et al., 2018). It is unclear whether these two grasslands in China have the same trends in PPT and whether the major climatic drivers are the same.

The PPT reflects the turning point in the vegetation photosynthesis dynamics from the greenup phase to the senescence phase. A shift in the PPT directly affects terrestrial carbon uptake during the peak season and consequently impacts annual carbon budgets and the seasonality of carbon cycle (Gonsamo et al., 2018; Wolf et al., 2016; Xu et al., 2016). In turn, these changes can alter the processes involved in the energy, water and nutrient cycles (Richardson et al., 2013; Zeng et al., 2017). The GPP<sub>annual</sub> of vegetation has experienced considerable interannual variation in the context of climate change (Anav et al., 2015). Recent studies have shown that the increase in vegetation productivity in warming northern regions is closely related to the advance in the PPT through enhanced carbon uptake early in the growing season (Gonsamo et al., 2018; Park et al., 2019; Xu et al., 2016). However, the consequences of changes in the PPT on carbon uptake vary among different regions (Park et al., 2019). For example, the correlation between an earlier peak and higher production is strong in some Arctic and boreal regions. Temperature stress in cold high latitudes can be alleviated due to warming, leading to an earlier SOS and PPT along with the increases in summertime peak production and annual production. In contrast, a relationship between an earlier peak and less production has been observed in some North American boreal forests and some temperate regions, mainly in water-limited ecosystems, where the PPT does not occur at the usual time due to water stress in summer, consequently influencing the peak and annual production (Angert et al., 2005; Buermann et al., 2013; Wang et al., 2018b; Wolf et al., 2016). These distinct impacts of PPT shifts on ecosystem productivity suggest a high degree of complexity in the climatic drivers in different regions and ecosystems (Park et al., 2019). In particular, whether the 'earlier PPT-higher production' pattern exists in the two typical grasslands in China (temperate and alpine) deserves further research (Gonsamo et al., 2018; Park et al., 2019).

In an effort to address the above-mentioned issues, the objective of this study is to examine the pattern and attribution of interannual variations in PPT, as well as the consequences of PPT shifts on GPP<sub>annual</sub> in typical temperate and alpine grasslands in China, by using improved data (remote sensing-based GPP products) and algorithms (gap-filling and fitting methods). Specifically, we attempt to answer three questions: (1) Do the PPT trends show consistent patterns between the temperate and alpine grasslands in China? (2) What are the main climatic drivers affecting the interannual variations in PPTs in the two grasslands? (3) How do the shifts in the PPT affect vegetation GPP<sub>annual</sub> in the two grasslands?

## 2. Materials and methods

### 2.1. Study area

The study area includes temperate grasslands (mainly located in Inner Mongolia and the Loess Plateau) with an average elevation of approximately 1200 m above sea level (ASL) and alpine grasslands (located in the Tibetan Plateau) with an average elevation of > 4000 m ASL (Fig. 1). Both of these grasslands are covered with herbs with distinct seasonality, but they have different plant species, climates and soil properties (Fan et al., 2016; Xu et al., 2016). In particular, the main

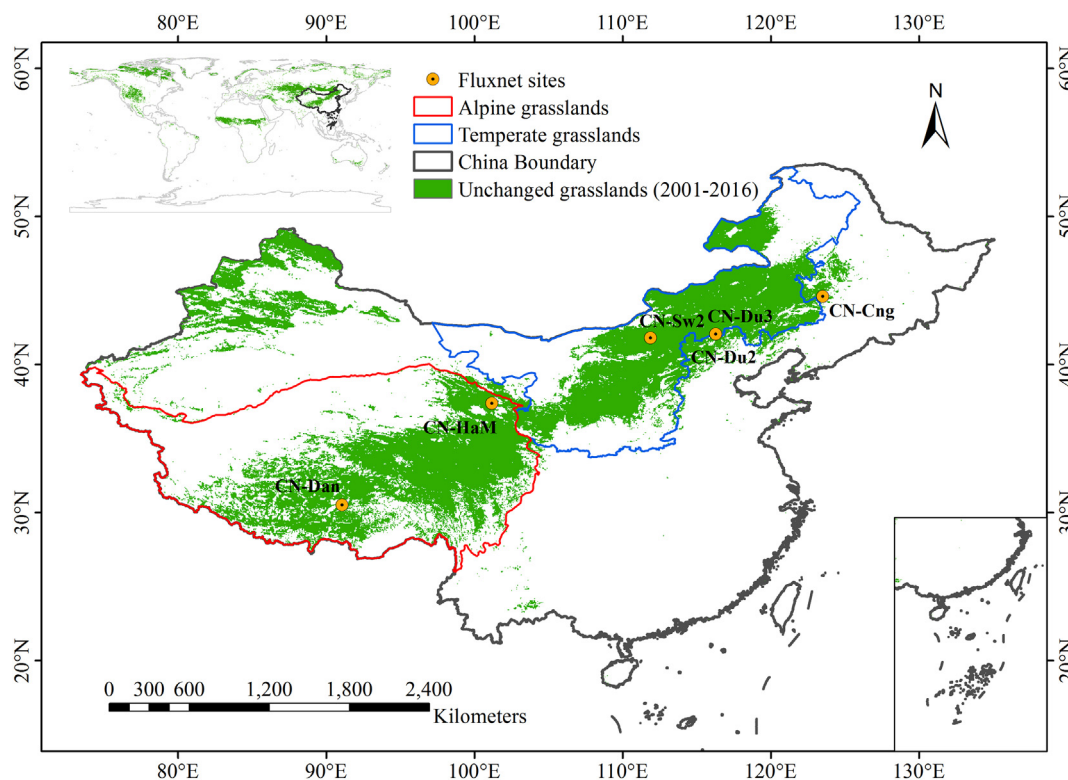


Fig. 1. Spatial distribution of temperate and alpine grasslands in China, including the Inner Mongolia Autonomous Region and Loess Plateau (referred to as the temperate grasslands) and the Tibetan Plateau (referred to as the alpine grasslands), and the locations of the FLUXNET tower sites used for validation in this study along the China Grassland Transect.

difference between the alpine grasslands and the temperate grasslands is that the former is characterized by a lower annual mean temperature, ranging from  $-15\text{ }^{\circ}\text{C}$  to  $5\text{ }^{\circ}\text{C}$  (Shen et al., 2015a; Liu et al., 2018; Wang et al., 2018c). In addition, pixels with a multiyear mean NDVI  $< 0.1$  were excluded to eliminate the impacts of sparsely vegetated areas (Shen et al., 2014b; Wu et al., 2018).

## 2.2. Data

### 2.2.1. GPP data at the eddy flux tower sites

Daily GPP ( $\text{GPP}_{\text{EC}}$ ) data from six eddy-covariance (EC) flux tower sites (13 site-years) in the FLUXNET 2015 database (<https://fluxnet.fluxdata.org>) were used (Table S1), including four temperate grassland sites (CN-Cng, CN-Du2, CN-Du3, and CN-Sw2) and two alpine grassland sites (CN-HaM and CN-Dan) (Yu et al., 2008; Yu et al., 2013).

### 2.2.2. GPP data products from the data-driven models

The satellite-based GPP data derived from the VPM model ( $\text{GPP}_{\text{VPM}}$ ) were used in this study to determine the phenological indices, including SOS and PPT. We used the 8-day  $0.05^{\circ}$  VPM GPP V2.0 dataset from 2000 to 2016 which was produced by simulations of an improved VPM model (Xiao et al., 2004a; Xiao et al., 2004b), the Moderate Resolution Imaging Spectroradiometer (MODIS) images, and the NCEP (National Centers for Environmental Prediction) Reanalysis II climate data (Zhang et al., 2017). This  $\text{GPP}_{\text{VPM}}$  product had two major improvements: first, it better captures the seasonal dynamics of vegetation by gap-filling low-quality or missing observations with a novel gap-filling and smoothing algorithm. Second, this product employed plant function type (PFT)-specific parameters for C3 and C4 plants (Zhang et al., 2017). The  $\text{GPP}_{\text{VPM}}$  product was assessed against GPP data from 113 EC flux towers around the globe, and the results showed good accuracy in terms of seasonal dynamics and interannual variation across biome types (Zhang et al., 2017). We also used other independent gridded GPP

products, including the FLUXCOM GPP products ( $\text{GPP}_{\text{FLUXCOM}}$ ) (Jung et al., 2017) and BESS GPP products ( $\text{GPP}_{\text{BESS}}$ ) (Jiang and Ryu, 2016; Ryu et al., 2011). The daily  $\text{GPP}_{\text{FLUXCOM}}$  with a spatial resolution of  $0.5^{\circ}$  was averaged from three machine learning algorithms (random forests, artificial neural networks, and multivariate adaptive regression splines) for 2000–2013. The  $\text{GPP}_{\text{FLUXCOM}}$  product was produced from 224 flux tower sites and combined with grid CRUNCEPv6 climate forcing data and satellite-based vegetation indices (VIs) data tiled by PFT as model-driving inputs (Jung et al., 2017). The  $\text{GPP}_{\text{BESS}}$  product with a 1-km resolution and 8-day interval from 2000 to 2015 was derived from the BESS model. The BESS model is a simplified remote sensing-derived biophysical process model that couples atmosphere and canopy radiative transfers, canopy photosynthesis, transpiration, and energy balance with multiple satellite remote sensing datasets (Jiang and Ryu, 2016). The BESS model used a mechanistic Farquhar model (an enzyme kinetic model) to estimate GPP, and the model has been proven to perform well in estimating GPP (Ryu et al., 2011).

### 2.2.3. MODIS surface reflectance product

The 17-year (2000–2016) MOD09A1 surface reflectance product with a spatial resolution of 500 m and an 8-day temporal interval was used to calculate the NDVI and Enhanced Vegetation Index (EVI) of the pixels that matched the coordinates of the above grasslands FLUXNET sites across China. The NDVI and EVI were calculated as follows (Huete et al., 2002).

$$\text{NDVI} = \frac{\rho_{\text{NIR1}} - \rho_{\text{RED}}}{\rho_{\text{NIR1}} + \rho_{\text{RED}}} \quad (1)$$

$$\text{EVI} = 2.5 \times \frac{\rho_{\text{NIR1}} - \rho_{\text{RED}}}{\rho_{\text{NIR1}} + 6 \times \rho_{\text{RED}} - 7.5 \times \rho_{\text{BLUE}} + 1} \quad (2)$$

where  $\rho_{\text{BLUE}}$ ,  $\rho_{\text{RED}}$ , and  $\rho_{\text{NIR1}}$  are the reflectance values from the blue (459–479 nm), red (620–670 nm), and NIR1 (841–875 nm) bands, respectively.

#### 2.2.4. MODIS land cover data

We used the grassland data layer from the MODIS Terra/Aqua Combined Land Cover Type Yearly product (MCD12C1 Version 6) with a spatial resolution of  $0.05^\circ$  and the International Geosphere-Biosphere Program (IGBP) classification scheme (Friedl and Sulla-Menashe, 2015). To ensure consistency in the land cover over the years, we selected those pixels that were classified as grassland in all years of 2001–2016.

#### 2.2.5. Gridded climate and soil moisture data

Gridded monthly temperature, precipitation, and downward short-wave radiation data with a spatial resolution of  $0.1^\circ$  over 2000–2016 were obtained from the China Meteorological Forcing Dataset (Chen et al., 2011; Yang et al., 2010). The climate dataset was derived from several existing international common meteorological datasets, including Princeton reanalysis data, GLDAS data, GEWEX-SRB radiation, and TRMM precipitation data (3B42), and the dataset was combined with China Meteorological Administration (CMA) station observation data (Chen et al., 2011).

The monthly soil moisture data were derived from the TerraClimate dataset, which has a monthly temporal resolution and a spatial resolution of  $1/24^\circ$  (Abatzoglou et al., 2018). The TerraClimate dataset uses climatically aided interpolation and combines high-spatial resolution climatological normals from the WorldClim dataset with data from CRU Ts4.0 and the Japanese 55-year Reanalysis (JRA55) to produce a monthly dataset. Additionally, it uses a water balance model that incorporates reference evapotranspiration, precipitation, temperature, and interpolated plant extractable soil water capacity (Abatzoglou et al., 2018).

### 2.3. Methods

#### 2.3.1. New algorithm for estimating SOS and PPT from multisource GPP products

We proposed a new framework for estimating SOS and PPT, that is, the hybrid generalized additive model (HGAM) method (Fig. S1). The HGAM includes a data gap-filling approach involving the modified Savitzky-Golay filter (Chen et al., 2004) (Fig. S2) and a data smoothing approach involving the generalized additive model (GAM) (Daniel and Charlie, 2018). As an adaptive nonparametric fitting method, the GAM algorithm represents the relationship between a response variable (e.g., GPP) and explanatory variables (e.g., day of year (DOY)) as a sum of smoothed link functions of the explanatory variables and uses penalized regression splines to obtain optimal fitting parameters (Hastie and Tibshirani, 1990). The smoothed link functions include three classes of smoothers, i.e., local regression (e.g., loess), smoothing splines and regression splines (e.g., B-splines, P-splines, and thin plate splines), to uncover hidden patterns in the data and fit the data with different patterns more appropriately (Hastie and Tibshirani, 1990; Larsen, 2015). Therefore, the HGAM algorithm is expected to be suitable for different GPP curves with asymmetric peaks or short plateaus during the peak season (Fig. S3).

Then, we applied the HGAM method on remote sensing-based GPP (i.e.,  $GPP_{VPM}$ ,  $GPP_{BESS}$ , and  $GPP_{FLUXCOM}$ ), NDVI, EVI, and flux site-based GPP (i.e.,  $GPP_{EC}$ ) time series to estimate the SOS and PPT. Different GPP products were used to ensure the robustness of the results. The specific technical process was as follows.

1) *Gap-filling and smoothing of the time series data.* The missing values and anomalies in raw GPP/NDVI/EVI time series were filled using the cubic spline interpolation and the modified Savitzky-Golay filter (Chen et al., 2004). This filtering step could make the input data into the following fitting model more stable and reasonable (Fig. S2). The integration of the two filters is more necessary when using NDVI and EVI as input. Next, the GAM fitting method was performed to smooth the above gap-filled GPP/NDVI/EVI to the daily GPP/NDVI/

EVI curve. For a more detailed description of the algorithm justification, please see the Supplementary Text S1.

2) *Estimates of SOS and PPT.* The SOS and PPT were estimated from the reconstructed daily GPP/NDVI/EVI curve. Specifically, the SOS was identified as the first day (DOY) when the reconstructed daily GPP/NDVI/EVI crossed a predefined threshold. Here we set the threshold to 10% of the multiyear average of amplitude in the seasonally smoothed GPP/NDVI/EVI curve for each pixel in 2000–2016 and for each validation flux tower site in all the available years (Shang et al., 2017; Wu et al., 2013; Zhou et al., 2016). The PPT was identified as the first day (DOY) when the fitted daily GPP/NDVI/EVI reached the peak (Xu et al., 2016) (Fig. S1).

#### 2.3.2. Evaluation of estimated PPT at flux tower sites

To evaluate the robustness of the estimated PPT from GPP, the following two methods were carried out.

- 1) Comparisons of PPTs extracted using the HGAM method with those using other fitting methods based on VPM GPP at flux tower sites. The other fitting methods included four common DLF fitting methods by Gonsamo et al. (2018), Elmore et al. (2012), Beck et al. (2006) and Gu et al. (2009). These four methods are referred to as Gonsamo's method, Elmore's method, Beck's method and Gu's method in this study. The PPT estimation with these methods was the same as with the HGAM method, except that the fitting method was replaced by the corresponding DLF method.
- 2) Comparisons of the interannual variance in PPT estimated from VPM GPP with that from independent MODIS NDVI and EVI data at flux tower sites. These comparisons were performed to determine whether the PPT derived from  $GPP_{VPM}$  data could capture the interannual variations in PPT. The method of PPT retrieval based on MODIS NDVI and EVI data was the same with that for the GPP product, but a step needed to be implemented in advance to replace the reduced NDVI/EVI values in nongrowing seasons with the median values over 2000–2016. This process further eliminated the effects of clouds or snow cover on NDVI and EVI following the procedures mentioned in the previous study (Shen et al., 2015a).

#### 2.3.3. Trend and variability analyses of PPT estimates

We examined the trend and interannual variability of PPT dynamics at the pixel and regional scales. First, we applied the Theil-Sen slope estimator combined with the Mann-Kendall test method to the PPT time series in each pixel to obtain the temporal trend and significance level of PPT over 2000–2016. The Theil-Sen slope estimator is a median-based non-parametric trend test estimator, which has no strict requirement in terms of data distribution. The Mann-Kendall test is a non-parametric trend test method, commonly employed to detect monotonic trends in time series related to geography (Forkel et al., 2015; Wang et al., 2018a). The trend analysis was also applied in the regional statistics in the temperate and alpine grasslands. The *t*-test based on pixels contained in the two studied grasslands was used to test whether there was a significant difference in the trends of PPT between the two regions.

Second, to obtain the dynamics of the interannual variability in the PPT, the standard deviation ( $STD_{PPT}$ ) was calculated after applying a 7-year moving window with a one-year lag at the pixel scale (Piao et al., 2014). After the  $STD_{PPT}$  values were calculated within each 7-year window, they were used in the above trend analysis method to assist in investigating the direction of the PPT variabilities over 17 years (Shi et al., 2018). In addition, moving-window analyses with different moving windows ranging from 5 to 11 years with a one-year lag were performed to explore the robustness of our results.

#### 2.3.4. Attribution analyses of PPT estimates

The length of the pre-season for each climatic factor (temperature, precipitation, and downward solar radiation) or soil moisture was

determined by the following two steps. First, we separately calculated the Pearson correlation coefficients between PPT and the each of climatic factors and soil moisture calculated from periods ahead of the month for which the multiyear average PPT was being determined at intervals of 1 month (Liu et al., 2016b; Shen et al., 2015a). We only considered the climate during the first half of the growing season (the spring-summer period); hence, the maximum preseason length was set from the multiyear average SOS to the multiyear average PPT on the basis of previous studies (Liu et al., 2016b; Shen et al., 2015a; Xu et al., 2018). Second, we determined the preseason time span in which the maximum Pearson correlation coefficient (absolute value) between the PPT and each specific climatic factor and soil moisture as the preseason length for the individual drivers.

Subsequently, to explore the linkage between the PPT and each individual climatic factor and soil moisture while eliminating the effects of the other three factors, we calculated the partial correlation coefficients between the PPT and mean temperature, sum precipitation, sum solar radiation and mean soil moisture over the preseason period (Liu et al., 2016a; Liu et al., 2016b; Peng et al., 2013; Shen et al., 2015a). To ensure the robustness of the results, the Pearson correlation coefficients between regionally averaged values of PPT and those of each individual climatic factor and soil moisture were also calculated for the temperate and alpine grasslands, respectively. In addition, we calculated the Pearson correlation coefficients between the SOS and PPT at each pixel and region to investigate the relationship between them. All data processing and statistical analyses were conducted in Python version 2.7 (<https://www.python.org/>), and the significance levels in this study were estimated with a two-tailed test.

In addition, to avoid differences caused by disparate datasets, we integrated all the data, including GPP, climate, and soil moisture data, into the same geographical range with the same spatial resolution ( $0.1^\circ$ ) and a monthly temporal resolution for the attribution analyses of interannual variance in the estimated PPTs.

### 3. Results

#### 3.1. Evaluation of HGAM-based PPTs and intercomparison with other independent variables

The validation of GPP-based PPT estimates of the HGAM method and the four DLF methods using FLUXNET GPP as reference showed that the HGAM method outperformed the four DLF methods with higher  $R^2$  and much lower root mean square error (RMSE) values ( $R^2 = 0.66$ , RMSE = 6.56 days), while  $R^2$  were 0.59, 0.60, 0.55, 0.58, and RMSEs were 7.07, 6.93, 7.34, 7.27 days for Gonsamo's method, Elmore's method, Beck's method, and Gu's method, respectively (Fig. 2a-e). In addition, the PPT estimates derived from GPP<sub>VPM</sub> were more accurate than those from MODIS NDVI ( $R^2 = 0.48$ , RMSE = 9.60 days) and EVI data ( $R^2 = 0.49$ , RMSE = 12.59 days) (Fig. 2e-g). In terms of the interannual variation of PPT, the results consistently showed that the interannual variation of PPT could be captured quite well by the GPP<sub>VPM</sub> data over 2000–2016 at flux tower sites (Fig. 2h).

According to the temporal profiles of GPP<sub>EC</sub> and GPP<sub>VPM</sub> corresponding to the pixels of flux tower sites, we found that the GPP curves with an asymmetrical peak and short plateau in the annual cycle were common at most sites (Figs. S3, 3). Compared to the DLF methods, the HGAM method was able to better capture the trajectory of seasonal vegetation photosynthetic activities (e.g., GPP<sub>max</sub>, PPT, and SOS); however, there were no clear differences in interannual variation of PPT among all methods (Fig. 3). Compared to the DLF methods, the HGAM method worked more effectively for some cases (e.g., CN-Sw2) where the GPP curves had double peaks during the peak season in a single cycle, which was likely caused by disturbances such as drought (Fig. 3h, i). In contrast, not all DLF methods could extract PPT well in these cases, such as Gonsamo's and Beck's methods, and the estimated

PPTs were greatly divergent, with great differences (e.g., a half month) among different DLF methods.

#### 3.2. Divergent pattern of PPT changes in the temperate and alpine grasslands of China

Although the multiyear average PPTs in the temperate and alpine grasslands of China were mainly located in a similar range from DOY 200 to 240 (the end of June to the end of August), the distribution of multiyear averaged PPTs showed different patterns in the two grasslands (Fig. 4). In the temperate grasslands, the PPT had a two-peak distribution of multiyear average PPTs ranging from DOY 180 to DOY 240, with an average value of DOY 211 (Fig. 4c). The two peaks (DOY 205 and DOY 219) were located in the southwestern and northern parts of the temperate grasslands (Fig. 4a). However, the alpine grasslands showed a narrow one-peak distribution of multiyear average PPTs ranging from DOY 190 to DOY 235 with an average PPT of DOY 212, and the peak (DOY 210) was mainly located in the center and eastern parts of the alpine grasslands (Fig. 4c). These results showed that the multiyear averaged PPTs of the alpine grasslands over 2000–2016 were more uniform than those of the temperate grasslands.

In terms of the PPT trends, the temperate grasslands experienced an overall advancing PPT trend. The temperate grasslands with advanced PPT accounted for approximately 80.9% (27.7% statistically significant at  $p < 0.05$ ) of the total temperate grasslands pixels (Fig. 5a). In contrast, the alpine grasslands experienced a delayed PPT, and the alpine grasslands pixels with delayed PPT accounted for ~ 83.0% of the total alpine grasslands pixels (14.4% statistically significant) (Fig. 5a). The areas with significant PPT trends were generally situated in eastern Qinghai Province, northern Shaanxi Province and the east-central parts of the Inner Mongolia Autonomous Region (Fig. 5a). We found that the PPT trends between temperate and alpine grasslands were significantly different at the pixel scale ( $p < 0.01$ ,  $t$ -test, Fig. 5b). The regionally averaged PPTs in the temperate and alpine grasslands showed contrasting rates of change  $-0.684 \text{ day yr}^{-1}$  ( $p < 0.05$ ) and  $0.288 \text{ day yr}^{-1}$  ( $p = 0.158$ ), respectively (Fig. 5b). The divergent shifts in PPT were more evident if only the pixels with significant trends were considered (Fig. 5c). Additionally, a much larger amplitude (absolute values of the linear regression slope) of PPT changes occurred in the temperate grasslands than in the alpine grasslands. The divergent spatial patterns of PPT were also verified using the DLF method (e.g., Gonsamo's method) (Fig. S4) and the independent FLUXCOM GPP and BESS GPP datasets (Fig. S5). A similar pattern of PPT trend was also found when using the  $0.1^\circ$  VPM GPP products (Fig. S6a).

#### 3.3. Attribution of grassland PPT dynamics

##### 3.3.1. Effects of preseason climatic factors on PPT changes

In the temperate grasslands, the PPT was mainly controlled by the preseason temperature and precipitation (Fig. 6a, b). The PPT showed positive partial correlations with preseason temperature in > 62.3% of the temperate grassland area, and these correlations were significant in 22.3% of the total temperate grassland area ( $p < 0.05$ ). This area was mainly distributed in the central and eastern parts of the temperate grasslands (Fig. 6a). Although the area with significant positive partial correlations between preseason precipitation and PPT was smaller (19.2%) than that between preseason temperature and PPT, the area accounted for ~ 66.6% of the temperate grasslands and was mainly located in the eastern and southeastern parts of the temperate grasslands (Fig. 6b). Limited area (~ 6.8% and 3.3%) showed significant relationships between PPT and solar radiation and between PPT and soil moisture, respectively (Fig. 6c, d).

In the alpine grasslands, the PPT change was mainly controlled by the preseason temperature and soil moisture (Fig. 6). Positive partial correlations between temperature and PPT were found in > 60.0% of the alpine grasslands area, 13.2% of which exhibited statistically

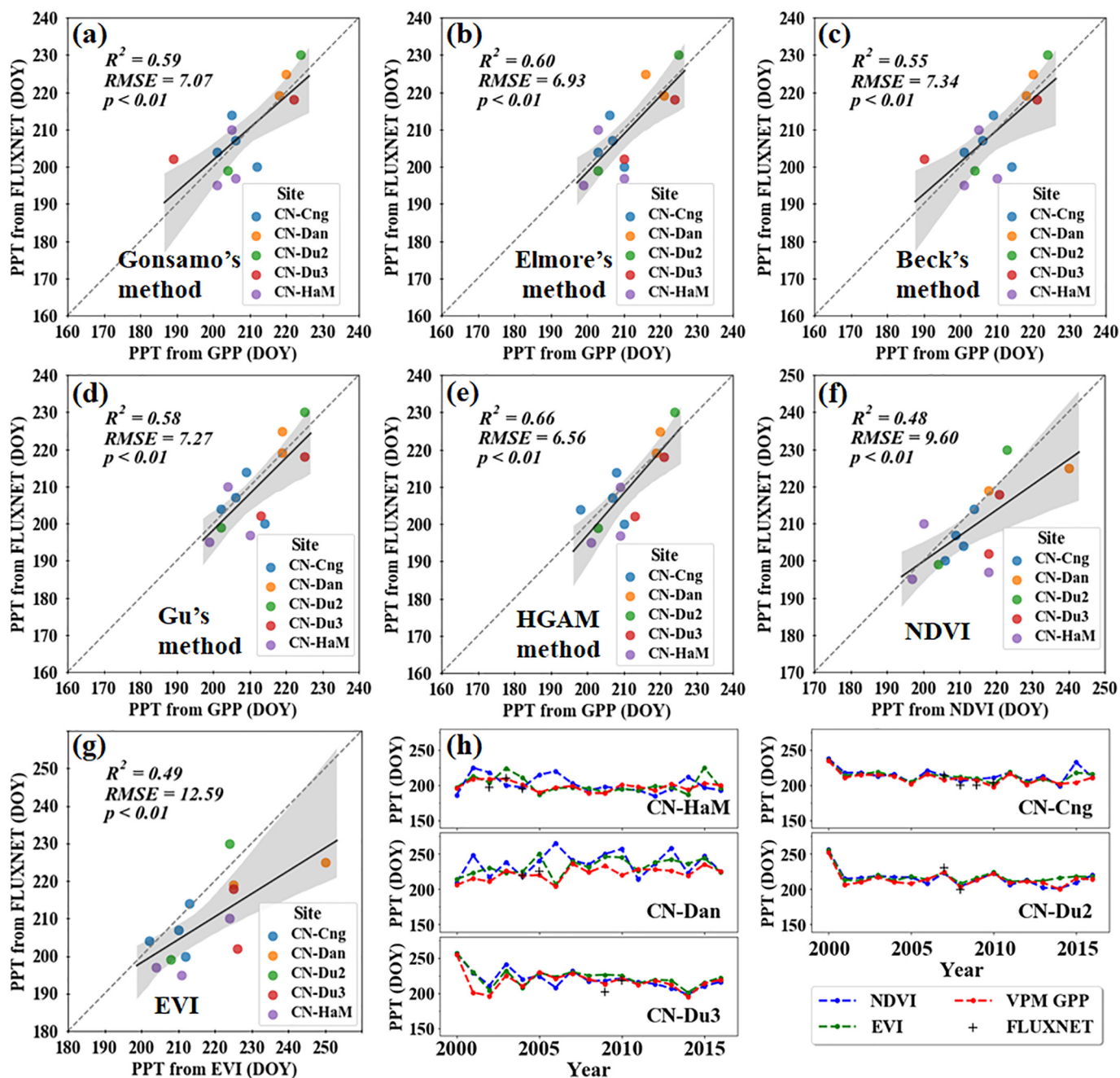


Fig. 2. Direct validation (a-e) and synergistic comparison (e-h) of peak photosynthesis timing (PPT) estimates based on different datasets and algorithms across flux sites in grasslands of China. Each data point in subfigures (a-g) represents a pair of PPT values derived from EC GPP and VPM GPP through (a) Gonsamo's method, (b) Elmore's method, (c) Beck's method, (d) Gu's method, and (e) HGAM method at the same site. The “CN-Sw2” site is not included due to the poor data quality in the raw time series. The light gray dotted line represents a 1:1 line. The black line is the estimated linear regression line. The shaded area represents the 95% confidence interval for the estimated black solid linear regression line. The label DOY denotes the day of year. The blue, green, and red dotted lines and the black symbols in subfigure (h) indicate the temporal profiles of PPT derived from MODIS NDVI, EVI, and VPM GPP and EC flux GPP, respectively, at six flux tower sites during 2000–2016. (For interpretation of the references to colour in this figure legend, the reader is referred to the web version of this article.)

significant correlations at  $p < 0.05$ . These areas mainly occurred in the central and southern parts of the Tibetan Plateau (Fig. 6a). The areas with partial positive correlations between soil moisture and PPT accounted for > 68.5% of the alpine grasslands (19.4% of which were statistically significant correlations) (Fig. 6c). Significant correlations between PPT and precipitation and between PPT and solar radiation also occurred in limited regions (7.5% and 8.0%, respectively) and were mainly distributed in the eastern and southern Tibetan Plateau (Fig. 6b, d).

These partial correlation results were confirmed by Pearson

correlation analysis at the pixel (Fig. S7) and regional levels (Fig. S8). In addition, both the partial correlation and Pearson correlation from the FLUXCOM GPP and BESS GPP, respectively, showed basically consistent results with those from the VPM model, although less area showed significant correlations for FLUXCOM GPP (Figs. S9-S12). The effect of soil moisture on PPT in the alpine grasslands was not well reflected in the analysis for FLUXCOM GPP.

### 3.3.2. Influence of spring phenology on changes of the PPT

A positive correlation between SOS and PPT was found in 80.7% of

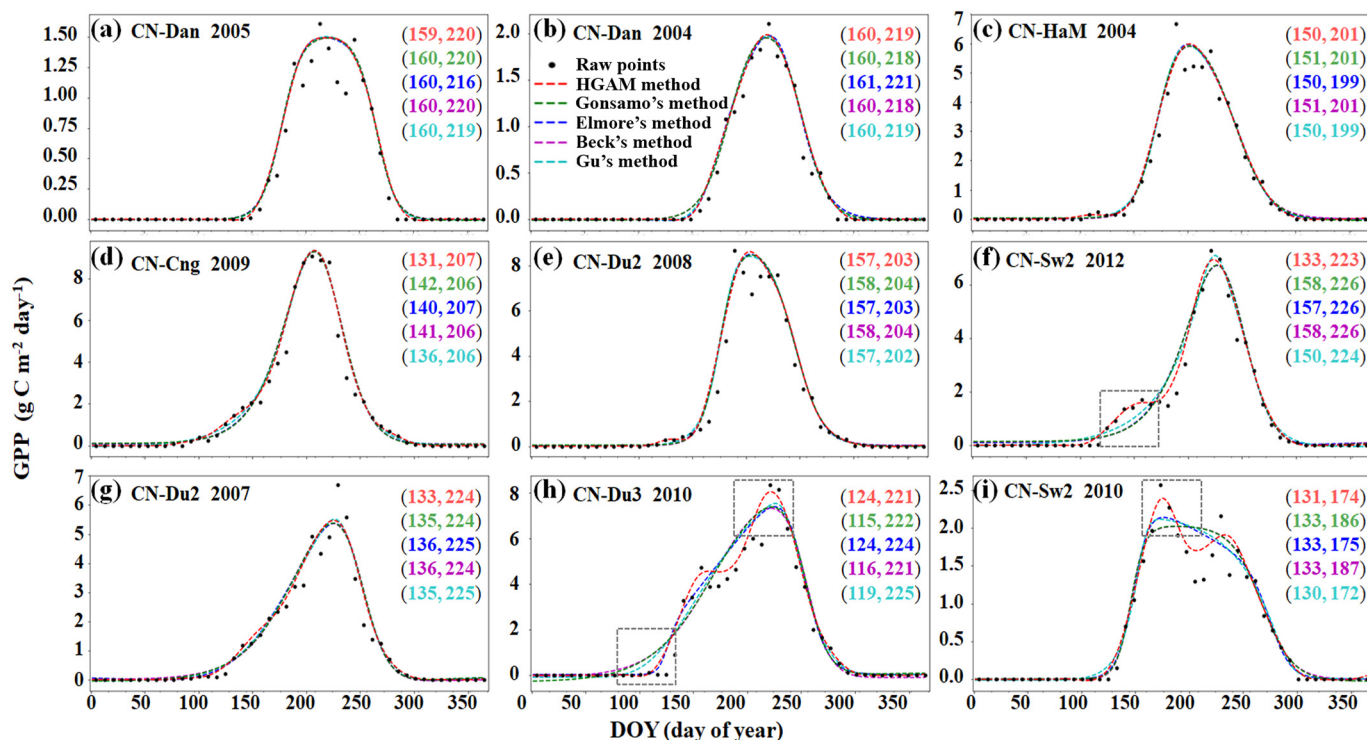


**Fig. 3.** The estimated phenology indices (SOS and PPT) derived from the hybrid generalized additive model (HGAM) method and four double logistic function (DLF) methods, respectively. SOS and PPT represent the start of the growing season and peak photosynthesis timing, respectively. The site-level case demonstrates that the HGAM approach can be used to estimate the PPT for VPM GPP with varied shapes at EC flux sites. The VPM GPP curves have symmetrical peaks (a), asymmetrical peaks and short plateaus (b-g) and asymmetrical double peaks (h-i), which first drop and then rise during the peak season (possibly caused by drought in summer). The black point indicates the original 8-day VPM GPP data. The red, green, blue, magenta and cyan dotted lines represent the fitted GPP curves derived from the HGAM approach and four DLF methods from Gonsamo et al. (2018), Elmore et al. (2012), Beck et al. (2006), Gu et al. (2009), respectively. The numbers in parentheses represent the estimated phenological indices (SOS and PPT), and the different colors represent the results of different methods, corresponding to the colors in the legend. (For interpretation of the references to colour in this figure legend, the reader is referred to the web version of this article.)

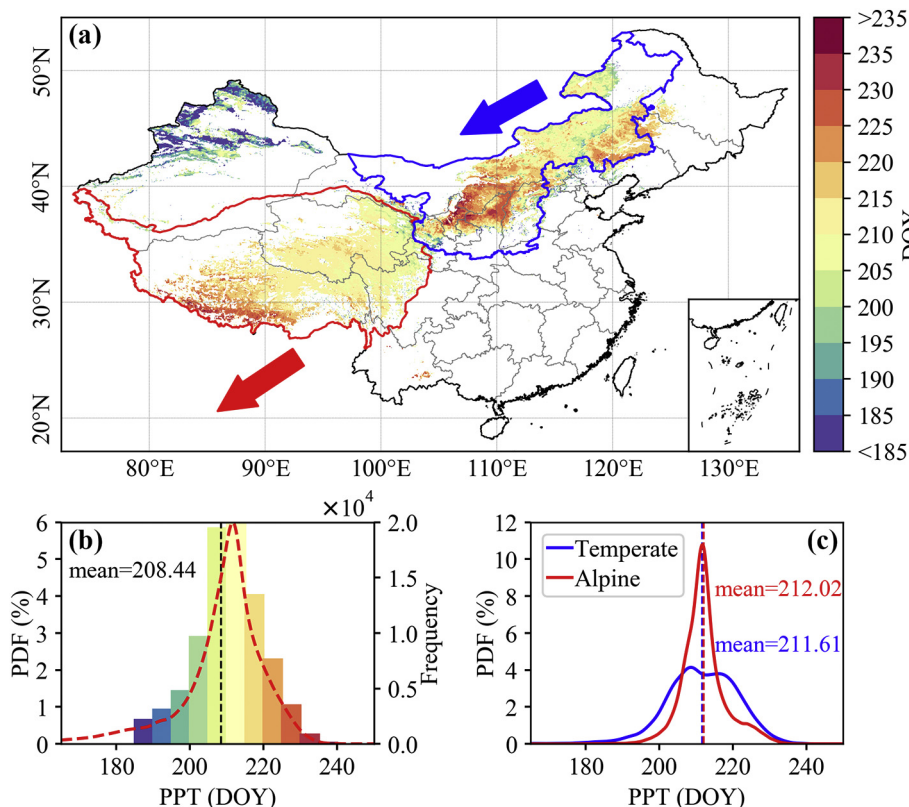


**Fig. 4.** Multiyear averaged peak photosynthesis timing (PPT) from the VPM-based GPP for grasslands in China. (a) The upper panel shows the spatial distribution of the 17-year averaged PPT for the grasslands in China. The bottom panel shows the frequency distribution of 17-year averaged PPT for (b) the all grasslands in China and (c) the temperate and alpine grasslands. The terms PDF and Frequency represent the probability density function and the frequency, respectively. DOY denotes the day of year. The blue outline indicates the temperate grasslands, and the red outline indicates the alpine grasslands. (For interpretation of the references to colour in this figure legend, the reader is referred to the web version of this article.)

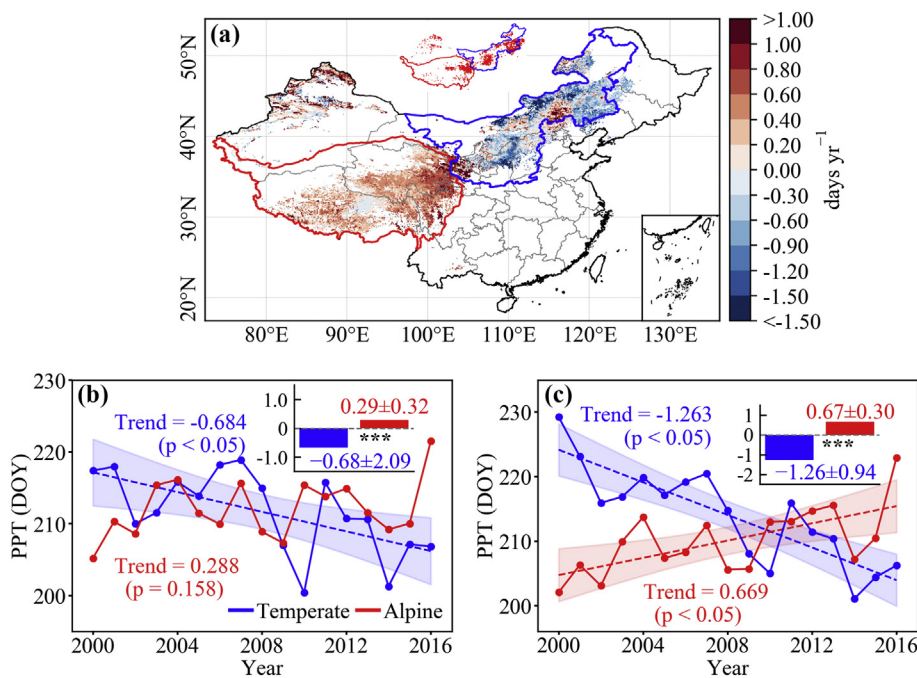


**Fig. 5.** The trends of peak photosynthesis timing (PPT) in the grasslands of China over the last 17 years (2000–2016). (a) The upper panel shows the spatial distribution of the trend and corresponding statistical significance of the 17-year PPT in the grasslands of China at the pixel scale. The red areas in the inset plot indicate that the trends are statistically significant ( $p < 0.05$ ). The bottom panels show the temporal trends of the regionally averaged 17-year PPTs in the temperate and alpine grasslands of China at the regional scale, i.e., (b) for entire grasslands and (c) for grassland pixels experiencing a significant trend. The dots connected by the solid lines represent the annual PPT values. The dashed lines represent the trend lines of the PPT changes. The shaded areas represent the 95% confidence interval of the estimated slope. The inset bar plots indicate the distributions (mean  $\pm$  1 standard deviation) of the PPT trends in these two regions. A significant difference in the trends of PPT exists between the two regions ( $p < 0.01$ ,  $t$ -test pixel-based). The blue colour indicates the temperate grasslands, and the red colour indicates the alpine grasslands. (For interpretation of the references to colour in this figure legend, the reader is referred to the web version of this article.)

the temperate and alpine grassland pixels, and the correlations were statistically significant at  $p < 0.05$  in 28.1% of the above two grasslands, mainly in the central and southern parts of the temperate grasslands and the southeastern part of the alpine grasslands (Fig. 7a). This positive correlation was also consistent with the analyses using the regionally averaged PPT and SOS values (Fig. 7b). However, the temperate and alpine grasslands showed different variations in the regionally averaged PPT and SOS (Fig. 7b, c). Specifically, the SOS and PPT showed a statistically significant consistency in interannual variation in the temperate grasslands ( $R = 0.70$ ,  $p < 0.05$ ), while the relationship between SOS and PPT in the alpine grasslands was insignificant ( $R = 0.07$ ,  $p > 0.05$ ).

### 3.4. Effects of PPT shifts on vegetation production

We found a significant increase in  $GPP_{\text{annual}}$  for both temperate and alpine grasslands (Fig. 8a), and the temperate grasslands had a higher growth rate of  $GPP_{\text{annual}}$  than that of the alpine grasslands (Fig. 8, c-f). The relationship between interannual variance in  $GPP$  and PPT also showed divergent patterns on pixel (Fig. 8b) and regional scales (Fig. 8c-f). Specifically, in the temperate grasslands, the increased  $GPP_{\text{annual}}$  had strong negative correlations with the earlier PPT ( $R = -0.58$ ,  $p < 0.05$ ) (Fig. 8c, e). In contrast, the insignificant positive correlation ( $R = 0.15$ ,  $p = 0.566$ ) between the increased  $GPP_{\text{annual}}$  and delayed PPT was shown in the alpine grasslands (Fig. 8d, f).

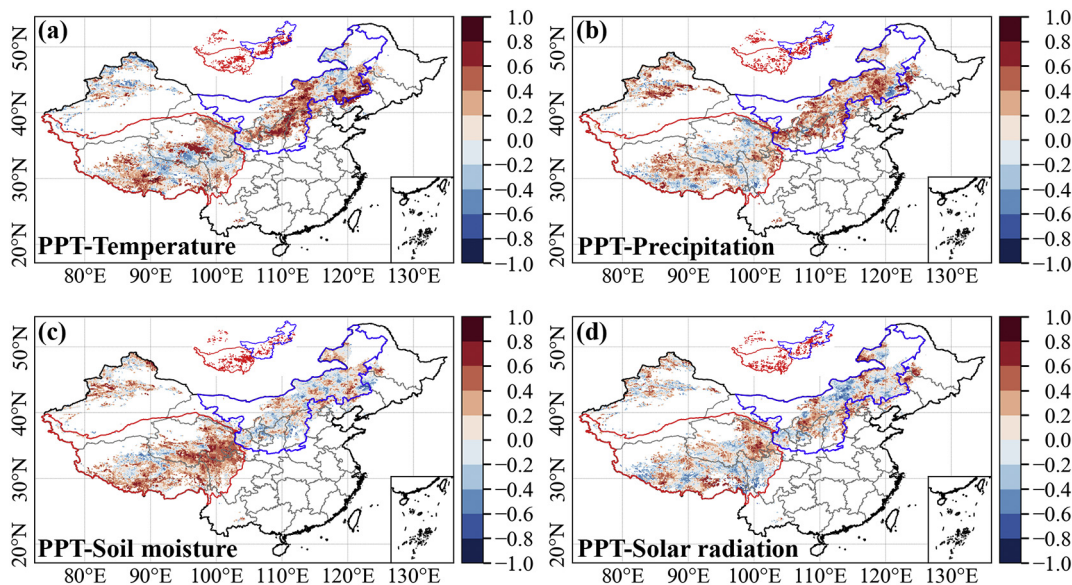


**Fig. 6.** Spatial patterns of partial correlation coefficients between peak photosynthesis timing (PPT) derived from VPM  $GPP$  and climatic factors, including pre-season temperature (a), precipitation (b), soil moisture (c) and downward solar radiation (d). The inset plots indicate the regions in which the corresponding partial correlations are significant at  $p < 0.05$ .

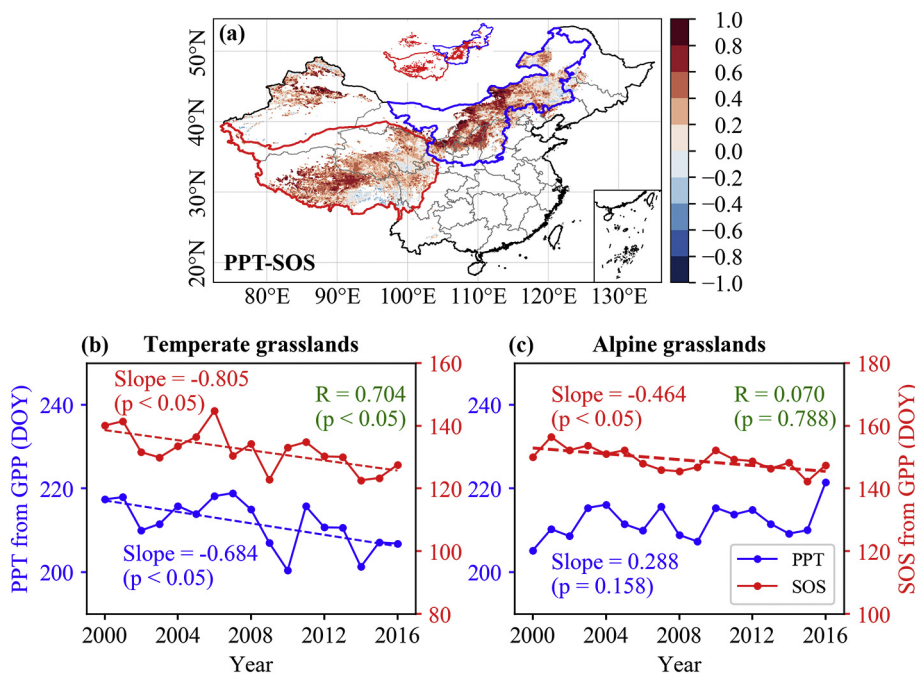


**Fig. 7.** Relationship between the spring phenology (start of the growing season, SOS) and peak photosynthesis timing (PPT). (a) The upper panel shows the spatial pattern of the Pearson correlation coefficients between SOS and PPT determined from VPM GPP with the hybrid generalized additive model (HGAM) method. The red area in the inset plot indicates the trends that are statistically significant ( $p < 0.05$ ). The bottom panels show the interannual variation and the corresponding relationships of the regionally averaged SOS and PPT in temperate grasslands (b) and alpine grasslands (c), including the areas where the correlation is insignificant ( $p > 0.05$ ). (For interpretation of the references to colour in this figure legend, the reader is referred to the web version of this article.)

## 4. Discussion

### 4.1. Improved HGAM framework for estimating the PPT

The consistent results from multiple independent datasets and four DLF fitting methods demonstrated the robustness of our newly proposed HGAM framework and the remote sensing-based GPP for monitoring the interannual variation in PPT (Figs. 2, S4, S5).

Generally, the photosynthetic responses of herbaceous plants fluctuated quickly in response to the changes in climate during the peak season within a single annual cycle; hence, GPP curves with asymmetrical peaks and short plateaus during the peak season were common in the grassland ecosystems (Fig. 3, S3). In the HGAM method, the fitting parameters and the type of eventually predictive functions do not need to be known in advance as the predictor functions can be automatically derived (Larsen, 2015). This can flexibly and automatically capture the spatiotemporal variations in phenological indices (e.g., SOS and PPT) and maximum GPP (Fig. 3 a-h) through several smooth functions (e.g., regression splines and smoothing splines) (Larsen, 2015). Therefore, the HGAM framework can provide more reliable gap-filling and data smoothing solutions for extracting land surface phenology, comparing to the existing parametric fitting methods.

During the peak season, there may be a specific shape of the GPP curve with two peaks, induced by a decline in GPP caused by disturbances such as drought and the subsequent recovery process (Fig. 3h) (Zhang et al., 2003). The DLF fitting methods smooth out most of these values during this period to achieve the global optimum of the fitting, which leads to overfitting (i.e., a flat peak), ignoring these normal real changes during this period. This problem is most pronounced in coarse-resolution remote sensing data (Gonsamo et al., 2018). In contrast, the GAM can tackle the bias/variance tradeoff in the constraint optimization and prevent this overfitting by automatically controlling the smoothness of the predictor functions (Larsen, 2015). Unlike the DLF methods, the shapes of GPP curves are fully determined by the data in the GAM, which can allow for more flexible and stable estimations of the various types of GPP curves. As the frequency and intensity of extreme events (such as droughts and heat waves) increase in the future (Zhang et al., 2016b), the cases in which the GPP curve exhibits two peaks during the peak season may increase. Our HGAM framework has a bigger potential in such situations than the DLF

methods.

The HGAM method was also expected to work for phenological metrics extraction of NDVI/EVI time series. The Savitzky-Golay filter, as the first step of HGAM framework, was well established for dealing with negative NDVI biased by clouds, cloud shadows, and aerosol (Chen et al., 2004); the GAM fitting method could also effectively capture the intra- and interannual changes of NDVI/EVI in plant growth using the flexible and accurate fitting functions mentioned above (Fig. 2h).

### 4.2. Divergent patterns in PPT shifts in the temperate and alpine grasslands

Although there were some differences in terms of magnitude of the PPT trends and the areas with significant PPT trends among the different methods and GPP products, the results consistently indicated that the PPT trends of temperate and alpine grasslands were different. The springward shift in PPT in the temperate grasslands was confirmed by two recent studies that mainly focused on northern areas ( $> 30^{\circ}\text{N}$ ) (Gonsamo et al., 2018; Park et al., 2019). Despite the insignificant trend of spatially averaged PPTs in the alpine grasslands, we still find a delay in the seasonality of photosynthesis hidden in the overall advance in the PPT in the northern alpine grasslands. For example, the northeastern part of the Tibetan Plateau has shown a significant autumnward shift in PPT. Nevertheless, the magnitudes of the PPT trends in temperate ( $-6.8$  days decade $^{-1}$ ) and alpine grasslands ( $2.9$  days decade $^{-1}$ ) in our study were greater than the previously reported ones in the northern ecosystems ( $1-2$  days decade $^{-1}$ ) (Gonsamo et al., 2018; Park et al., 2019; Xu et al., 2016) (Fig. 5). The differences in slope magnitudes may be due to the faster warming in the Inner Mongolia Plateau ( $0.35$   $^{\circ}\text{C}$  decade $^{-1}$ ) and Tibetan Plateau ( $0.16$   $^{\circ}\text{C}$  decade $^{-1}$ ) than over the northern hemisphere ( $0.05$   $^{\circ}\text{C}$  decade $^{-1}$ ) over the past few decades (Liu et al., 2018), suggesting large spatial differences or gradients in PPT dynamics exist among different geographic areas, even within the same land cover type (i.e., grassland).

Despite the divergent patterns of PPT in the temperate and alpine grasslands, both temperate grasslands and alpine grasslands showed consistent increases in the variabilities in annual PPT from 2000 to 2016 at the pixel and regional scales (Fig. 9). Specifically, the trend analysis of the PPT standard deviations within 7-year moving windows showed a significant increase in the interannual variability in PPT in most of the temperate and alpine grasslands (Fig. 9). Consistent

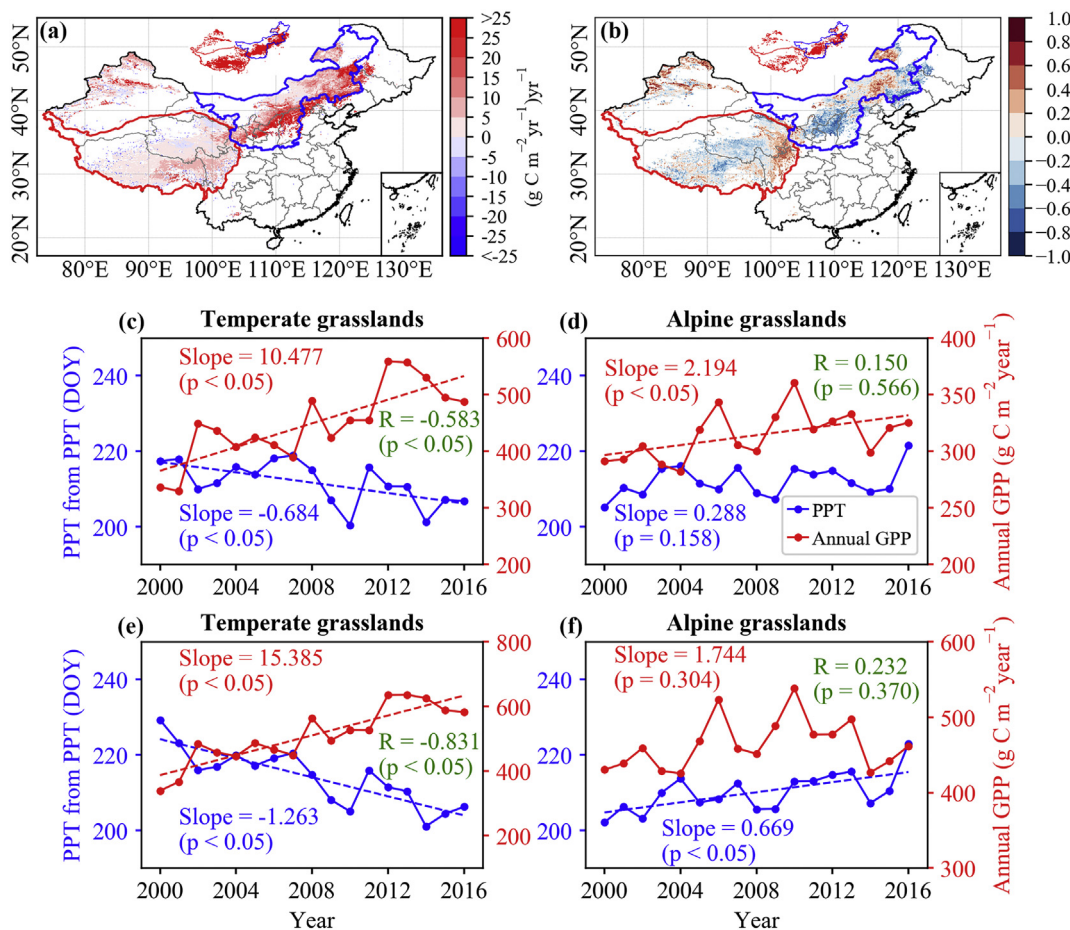


**Fig. 8.** The spatial pattern of the relationship between peak photosynthesis timing (PPT) and annual GPP in the grasslands of China during 2000–2016 at the pixel and regional scales. (a) The trend of annual GPP was determined by VPM GPP in the temperate and alpine grasslands of China. (b) The spatial pattern of the Pearson correlation coefficients between annual GPP and PPT was derived from VPM GPP with the hybrid generalized additive model (HGAM) method. The red area in the inset plot indicates the trends that are statistically significant ( $p < 0.05$ ). The middle panels show the interannual variation and the corresponding relationship of the regionally averaged PPT and annual GPP for the temperate grasslands (c) and alpine grasslands (d), regardless of the significance level of the PPT trend. The bottom panels show the interannual variation and relationship for the areas with significant PPT trends ( $p < 0.05$ ) in the temperate grasslands (e) and alpine grasslands (f). The green colour indicates the Pearson correlation coefficients and corresponding significance between PPT and annual GPP for each grassland type. (For interpretation of the references to colour in this figure legend, the reader is referred to the web version of this article.)

patterns were observed in the analyses with different moving-window lengths in the range from 5 to 11 years (Fig. S13). This finding could explain why the areas with significant trends were limited (Fig. 5).

#### 4.3. Synergistic effects of climate and spring phenology on shifts of PPT in different grasslands

The pre-season temperature plays a consistent controlling role in regulating PPT changes among climatic factors (Fig. 6), which was consistent with previous studies (Park et al., 2019; Xu et al., 2016). Interestingly, precipitation and soil moisture have some regulatory impacts in temperate and alpine grasslands, respectively. In water-limited temperate grasslands, warming-induced enhancements in evapotranspiration likely lead to the earlier-than-normal consumption of soil water. Therefore, within the background of reduced temperature and increased precipitation in the pre-season (Fig. S14), peak photosynthesis of plants occurs earlier to benefit from the relatively high precipitation and mild temperature in the late spring or early summer (Maseyk et al., 2010; Park et al., 2019; Schimel, 2010; Xu et al., 2016). Meanwhile, limited precipitation cannot replenish soil water in a timely and effective manner. The subsequent soil water deficit hinders plant growth by reducing the plant maximum photosynthetic rate, consequently leading to an earlier PPT (Hufkens et al., 2016; Liu et al., 2018).

This earlier PPT occurrence of temperate vegetation has been considered an ecophysiological acclimation that enables vegetation to optimize growth before the warmer and drier summer (Schimel, 2010).

In contrast, recent warming in the alpine grasslands did not lead to an insufficient chilling requirement (Fu et al., 2015; Shen et al., 2015b), and the higher pre-season temperature played a continuously positive role in plant photosynthesis. The bioactivity of a variety of enzymes for photosynthetic and dark reactions requires an appropriate temperature (Fu et al., 2014). Several previous efforts have also shown that warming-induced greening (Keenan and Riley, 2018) or PPT advance (Park et al., 2019) in cold, high-latitude ecosystems is associated with a continuous release of temperature limitations on photosynthetic activities. Increasing the pre-season temperature enhances photosynthesis due to a warming-stimulated increase in the optimum temperature of plant photosynthesis (Huang et al., 2019), consequently delaying the time at which plants reach peak photosynthesis (Liu et al., 2018). Compared to temperature, the effect of precipitation on PPT was not significant on the Tibetan Plateau. Although precipitation had some effect on PPT in limited regions (e.g., northeastern region), permafrost is a critical water source affecting soil moisture in the alpine grasslands (Chen et al., 2013). Warming-induced processes in soil enhance the melting of permafrost, which likely replenishes depleted soil moisture in the root zone of plants and counteracts excessive plant transpiration

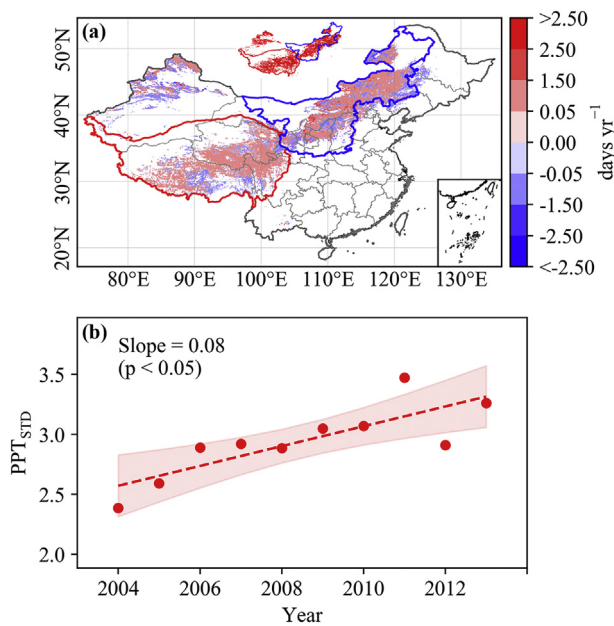


**Fig. 9.** The pattern of linear trend in the variabilities of PPT from 2000 to 2016 at pixel and region scales. (a) The upper panel shows the spatial distribution of the linear trend of the standard deviations of PPT within the 7-year windows. The red marked area in the inset plot indicates the regions with statistical significance ( $p < 0.05$ ). (b) The bottom panel shows the trend of the standard deviations of spatially averaged PPT within the 7-year windows in both temperate and alpine grasslands. The year on the horizontal axis is the central year of the 7-year sliding window that represents the corresponding period (e.g., 2003 refers to the sliding window from 2000 to 2006). (For interpretation of the references to colour in this figure legend, the reader is referred to the web version of this article.)

and soil evaporation due to rising temperatures. Moreover, surplus water in the previous year is usually stored in the deep soil layer and can reduce the soil water deficit in the following drought season through the hydraulic lifting of the roots and the conversion of capillary water. These results may also explain why changes in PPT did not respond to precipitation in some areas of the alpine grasslands, and these relationships can be further explained by the correlation between soil moisture and PPT in the alpine grasslands (Fig. S8 c;  $R = 0.63$ ,  $p < 0.05$ ).

Interestingly, the biological properties of plants are also considerable factors influencing PPTs in addition to climatic factors. The positive and significant relationships between SOS and PPT at both the pixel and regional scales in our study (Fig. 7) was consistent with the results of a recent satellite-based study (Gonsamo et al., 2018), that is, an earlier SOS tends to translate into an earlier PPT. A similar relationship also exists between the SOS and EOS according to previous studies (Fu et al., 2014; Liu et al., 2016b). This pattern could be explained by the following two aspects. The first reason is likely the internal self-regulated mechanism of vegetation, which controls individual plant development at the genetic, molecular, and individual levels. Specifically, the programmed apoptosis mechanism of cells (Lim et al., 2007) and leaf life span (Reich et al., 1992) will not allow the highly active photosynthesis of plants to continue to carry on. Second, the SOS affects subsequent phenological phases by influencing the environmental conditions in spring and summer (Fu et al., 2014). Specifically, advances in the leaf-out period can lead to premature soil moisture losses (Buermann et al., 2013; Fu et al., 2018). Earlier SOS can lead to an advance in drought events in the prosperous period and a decrease in peak production, which subsequently causes an advance in the PPT. Therefore, there may be a connection between spring and summer phenology, and this effect of spring phenology on peak vegetation phenology has remarkable implications for understanding and

modeling vegetation phenology (Buermann et al., 2018).

#### 4.4. Consequences of PPT shifts on annual production in both grasslands

The dynamics of PPT explicitly affect the spatiotemporal pattern of vegetation photosynthetic activity under climate change (Fu et al., 2014), subsequently affecting annual production ( $GPP_{\text{annual}}$ ) of grasslands (Park et al., 2019). Consistent with Park et al. (2019), our study indicated that the changes in PPT could cause different impacts on  $GPP_{\text{annual}}$ , and these effects would depend on different climate and soil moisture constraints on plant growth (Fig. 8). We verified that the earlier peak-higher production pattern did exist in the temperate grasslands, agreeing with a previous study (Gonsamo et al., 2018). In these circumstances, the earlier onset of carbon uptake was strongly linked to an earlier onset of peak photosynthesis and higher  $GPP_{\text{annual}}$  (Fig. 8). Based on the findings of a previous study, the risk of water deficit and productivity decline is more likely to occur in the temperate region, especially in regions where warmer and drier conditions are dominant (Park et al., 2019). However, the MODIS-based earlier peak-less production pattern found in warmer temperate vegetation of the northern hemisphere is not explicitly reflected in our study (Park et al., 2019).

In the case of warming in alpine grasslands, the advance of the SOS did not cause earlier PPT but still led to an increase in  $GPP_{\text{annual}}$ , suggesting that there may be another mechanism to interpret the inter-annual changes of vegetation productivity in the alpine grasslands. This possible later peak-higher production pattern can be clearly seen in alpine grassland areas where the PPT was significantly delayed (Figs. 5, 8b). The pattern may be more related to the lengthening of the growing season than the increased maximum photosynthetic rate, thereby leading to an increase in production. These findings in our study are important for understanding the possible mechanism of interannual variance in  $GPP_{\text{annual}}$ .

#### 4.5. Uncertainties and implications

Due to the limitation in the number of available flux tower sites in the study area, only 13 site-years of data were used for the validation of PPT. Additionally, the limitation in the length of the study period may also be a source of uncertainty (Wang et al., 2019). Therefore, the increasing amount of flux tower data used in the future could help to further refine and calibrate the algorithm of PPT extraction.

In terms of the  $GPP_{\text{VPM}}$ ,  $GPP_{\text{BESS}}$  and  $GPP_{\text{FLUXCOM}}$  products, there are some differences in the magnitudes of the estimated PPT trends and the areas with significant PPT trends. The reason may be due to differences in the models, the input data and the resolutions (Ryu et al., 2019). These uncertainties and gaps among existing GPP products imply that the GPP-based PPT can be treated as an indicator for benchmarking the seasonality of simulated GPP in terrestrial biosphere models and remote sensing-based GPP models. In addition to GPP, the satellite-retrieved solar-induced chlorophyll fluorescence (SIF) data can also be used as a good proxy of photosynthesis due to the high sensitivity of the data and the good consistency with the ecosystem carbon flux (Song et al., 2018; Wagle et al., 2014; Zhang et al., 2016a). However, the extreme uncertainties in long-term and interannual variations in satellite-based SIF data caused by sensor degradation issues limit the application of these data at the regional scale (Ryu et al., 2019).

Moreover, the grazing and afforestation in the past two decades were the dominant human intervention practices on the temperate grasslands, whereas human-driven land use changes were not remarkable in the alpine grasslands. The  $0.05^\circ$  MODIS-based land cover maps used to define the grassland extent in this study inevitably include some shrubs. Therefore, the human intervention process and coarse grassland information could affect the results. In addition, changes in biodiversity may also be a factor that could potentially distort the PPT changes, and

such changes could change the vegetation types and/or the dominant herb communities, resulting in vegetation with different phenological characteristics.

This study suggests that climatic and biological factors coregulate the spatiotemporal dynamics of PPT in China's grasslands. Although significant correlations between climatic drivers and PPT trends were limited to quite small fractions of the total area, and temperate and alpine grasslands exhibit opposing patterns of change. Consequently, it is possible that the distinction of temperate vs. alpine grasslands cannot fully explain the observed patterns and the underlying situation is more complicated. Therefore, more factors, such as different vegetation types, topographic characteristics, and soil properties, could also affect the spatiotemporal pattern of vegetation peak photosynthesis across different biomes (Misra et al., 2018). Under the background of increasing extreme climate events (Zhou et al., 2017), a more comprehensive understanding of the shift in vegetation peak phenology needs more studies (Park et al., 2019). The divergent pattern observed between temperate and alpine grasslands in China is likely to open new lines of research into plant peak phenology and ecosystem functioning in grasslands and other vegetation types via remote sensing observations and field experiments, as well as model simulations on seasonal to decadal timescales.

## 5. Conclusions

In this study, a new HGAM method and the remote sensing-based VPM GPP product were applied to investigate the spatial and temporal patterns of PPT changes, their drivers, and their effects on annual GPP in China's grasslands from 2000 to 2016. The results showed that the temperate grasslands experienced a significant springward shift in PPT, whereas the alpine grasslands experienced an emerging delay in PPT. The interannual variations in PPT in most of the temperate and alpine grasslands were found to be positively associated with the pre-season temperature. In addition, positive correlations existed between pre-season precipitation and PPT in the temperate grasslands and between pre-season soil moisture and PPT in the alpine grasslands. Moreover, we found a positive influence of spring phenology (e.g., SOS) on PPT across grasslands in China, which revealed that spring phenology is also an important factor influencing PPT shifts. We verified that the earlier peak-higher production pattern existed in temperate grasslands but not in alpine grasslands in China. This study provides important implications for understanding the spatiotemporal dynamics of vegetation photosynthetic activity in response to climate change in different ecosystems and could contribute to benchmarking the seasonality of simulated production in terrestrial biosphere models. This study expects to shed light on the mechanism of peak vegetation activities and the improvement of terrestrial ecosystem models, especially the simulations of terrestrial carbon uptake.

## Acknowledgements

This study was supported by the National Key Research and Development Program of China (2018YFA0606101), the Strategic Priority Research Program (XDA19040301), the Key Research Program of Frontier Sciences (QYZDB-SSW-DQC005) of the Chinese Academy of Sciences (CAS), and the "Thousand Youth Talents Plan". We acknowledge all contributors of the FLUXNET Network (<http://fluxnet.fluxdata.org/>) for sharing the FLUXNET 2015 Dataset. We are grateful to the Earth Observation and Modeling Facility (EOMF) for providing the VPM GPP time series data (<http://www.eomf.ou.edu/>), Martin Jung and Gianluca Tramontana for sharing the FLUXCOM GPP data (<https://www.bgc-jena.mpg.de/geodb/projects/Home.php>), the Environmental Ecology Lab for providing the BESS GPP time series data (<http://environment.snu.ac.kr>), the Data Assimilation and Modeling Center for Tibetan Multi-spheres for providing the meteorological forcing dataset (<http://www.tpdatabase.cn/portal/index.jsp>), the Climatology Lab for

providing TerraClimate dataset (<http://www.climatologylab.org/terraclimate.html>). J. Y. gratefully acknowledges the China Scholarship Council for the financial support of a 24-month study at the University of Oklahoma.

## Appendix A. Supplementary data

Supplementary data to this article can be found online at <https://doi.org/10.1016/j.rse.2019.111395>.

## References

- Abatzoglou, J.T., Dobrowski, S.Z., Parks, S.A., Hegewisch, K.C., 2018. TerraClimate, a high-resolution global dataset of monthly climate and climatic water balance from 1958-2015. *Sci Data* 5, 170191.
- Anav, A., Friedlingstein, P., Beer, C., Ciais, P., Harper, A., Jones, C., Murray-Tortarolo, G., Papale, D., Parazoo, N.C., Peylin, P., Piao, S.L., Sitch, S., Viivy, N., Wiltshire, A., Zhao, M.S., 2015. Spatiotemporal patterns of terrestrial gross primary production: a review. *Rev. Geophys.* 53, 785–818.
- Angert, A., Biraud, S., Bonfils, C., Henning, C.C., Buermann, W., Pinzon, J., Tucker, C.J., Fung, I., 2005. Drier summers cancel out the CO<sub>2</sub> uptake enhancement induced by warmer springs. *Proc. Natl. Acad. Sci. U. S. A.* 102, 10823–10827.
- Beck, P.S.A., Atzberger, C., Högda, K.A., Johansen, B., Skidmore, A.K., 2006. Improved monitoring of vegetation dynamics at very high latitudes: a new method using MODIS NDVI. *Remote Sens. Environ.* 100, 321–334.
- Buermann, W., Bikash, P.R., Jung, M., Burn, D.H., Reichstein, M., 2013. Earlier springs decrease peak summer productivity in north American boreal forests. *Environ. Res. Lett.* 8, 024027.
- Buermann, W., Forkel, M., O'Sullivan, M., Sitch, S., Friedlingstein, P., Haverd, V., Jain, A.K., Kato, E., Kautz, M., Lienert, S., Lombardozzi, D., Nabel, J., Tian, H., Wiltshire, A.J., Zhu, D., Smith, W.K., Richardson, A.D., 2018. Widespread seasonal compensation effects of spring warming on northern plant productivity. *Nature* 562, 110–114.
- Chen, J., Jönsson, P., Tamura, M., Gu, Z., Matsushita, B., Eklundh, L., 2004. A simple method for reconstructing a high-quality NDVI time-series data set based on the Savitzky-Golay filter. *Remote Sens. Environ.* 91, 332–344.
- Chen, Y., Yang, K., He, J., Qin, J., Shi, J., Du, J., He, Q., 2011. Improving land surface temperature modeling for dry land of China. *J. Geophys. Res.* 116.
- Chen, H., Zhu, Q., Peng, C., Wu, N., Wang, Y., Fang, X., Gao, Y., Zhu, D., Yang, G., Tian, J., Kang, X., Piao, S., Ouyang, H., Xiang, W., Luo, Z., Jiang, H., Song, X., Zhang, Y., Yu, G., Zhao, X., Gong, P., Yao, T., Wu, J., 2013. The impacts of climate change and human activities on biogeochemical cycles on the Qinghai-Tibetan plateau. *Glob. Chang. Biol.* 19, 2940–2955.
- Daniel, S., Charlie, B., 2018. pyGAM: Generalized Additive Models in Python. Zenodo <https://doi.org/10.5281/zenodo.1208723>.
- Dong, J.W., Xiao, X.M., Wagle, P., Zhang, G.L., Zhou, Y.T., Jin, C., Torn, M.S., Meyers, T.P., Suyker, A.E., Wang, J.B., Yan, H.M., Biradar, C., Moore, B., 2015. Comparison of four EVI-based models for estimating gross primary production of maize and soybean croplands and tallgrass prairie under severe drought. *Remote Sens. Environ.* 162, 154–168.
- Elmore, A.J., Guinn, S.M., Minsley, B.J., Richardson, A.D., 2012. Landscape controls on the timing of spring, autumn, and growing season length in mid-Atlantic forests. *Glob. Chang. Biol.* 18, 656–674.
- Fan, J.W., Harris, W., Zhong, H.P., 2016. Stoichiometry of leaf nitrogen and phosphorus of grasslands of the inner Mongolian and Qinghai-Tibet plateaus in relation to climatic variables and vegetation organization levels. *Ecol. Res.* 31, 821–829.
- Forkel, M., Migliavacca, M., Thonicke, K., Reichstein, M., Schaphoff, S., Weber, U., Carvalhais, H., 2015. Codominant water control on global interannual variability and trends in land surface phenology and greenness. *Glob. Chang. Biol.* 21, 3414–3435.
- Friedl, M., Sulla-Menashe, D., 2015. MCD12C1 MODIS/Terra+ Aqua Land Cover Type Yearly L3 Global 0.05Deg CMG V006. NASA EOSDIS Land Processes DAAC.
- Fu, Y.S., Campioli, M., Vitasse, Y., De Boeck, H.J., Van den Berge, J., AbdElgawad, H., Asard, H., Piao, S., Deckmyn, G., Janssens, I.A., 2014. Variation in leaf flushing date influences autumnal senescence and next year's flushing date in two temperate tree species. *Proc. Natl. Acad. Sci. U. S. A.* 111, 7355–7360.
- Fu, Y.H., Piao, S., Vitasse, Y., Zhao, H., De Boeck, H.J., Liu, Q., Yang, H., Weber, U., Hanninen, H., Janssens, I.A., 2015. Increased heat requirement for leaf flushing in temperate woody species over 1980-2012: effects of chilling, precipitation and insolation. *Glob. Chang. Biol.* 21, 2687–2697.
- Fu, Y.Y., He, H.S., Zhao, J.J., Larsen, D.R., Zhang, H.Y., Sunde, M.G., Duan, S.W., 2018. Climate and spring phenology effects on autumn phenology in the Greater Khingan Mountains, northeastern China. *Remote Sens.* 10, 449.
- Garonna, I., de Jong, R., de Wit, A.J., Mucher, C.A., Schmid, B., Schaepman, M.E., 2014. Strong contribution of autumn phenology to changes in satellite-derived growing season length estimates across Europe (1982-2011). *Glob. Chang. Biol.* 20, 3457–3470.
- Ge, R., He, H.L., Ren, X.L., Zhang, L., Li, P., Zeng, N., Yu, G.R., Zhang, L.Y., Yu, S.Y., Zhang, F.W., Li, H.Q., Shi, P.L., Chen, S.P., Wang, Y.F., Xin, X.P., Ma, Y.M., Ma, M.G., Zhang, Y., Du, M.Y., 2018. A satellite-based model for simulating ecosystem respiration in the Tibetan and Inner Mongolian grasslands. *Remote Sens.* 10, 149.
- Gonsamo, A., Chen, J.M., Ooi, Y.W., 2018. Peak season plant activity shift towards spring is reflected by increasing carbon uptake by extratropical ecosystems. *Glob. Chang. Biol.* 24, 2117–2128.

- Gu, L., Post, W.M., Baldocchi, D.D., Black, T.A., Suyker, A.E., Verma, S.B., Vesala, T., Wofsy, S.C., 2009. Characterizing the seasonal dynamics of plant community photosynthesis across a range of vegetation types. In: Noormets, A. (Ed.), *Phenology of Ecosystem Processes: Applications in Global Change Research*. Springer New York, New York, NY, pp. 35–58.
- Hastie, T., Tibshirani, R., 1990. *Generalized Additive Models*. Chapman and Hall.
- Hegland, S.J., Nielsen, A., Lázaro, A., Bjerknes, A.L., Totland, Ø., 2009. How does climate warming affect plant-pollinator interactions? *Ecol. Lett.* 12, 184–195.
- Huang, M., Piao, S., Ciais, P., Penuelas, J., Wang, X., Keenan, T.F., Peng, S., Berry, J.A., Wang, K., Mao, J., Alkama, R., Cescatti, A., Cuntz, M., De Deurwaerder, H., Gao, M., He, Y., Liu, Y., Luo, Y., Myneni, R.B., Niu, S., Shi, X., Yuan, W., Verbeeck, H., Wang, T., Wu, J., Janssens, I.A., 2019. Air temperature optima of vegetation productivity across global biomes. *Nat. Ecol. Evol.* 3, 772–779.
- Huete, A., Didan, K., Miura, T., Rodriguez, E.P., Gao, X., Ferreira, L.G., 2002. Overview of the radiometric and biophysical performance of the MODIS vegetation indices. *Remote Sens. Environ.* 83, 195–213.
- Huete, A.R., Miura, T., Kim, Y., Didan, K., Privette, J., 2006. Assessments of multisensor vegetation index dependencies with hyperspectral and tower flux data. In: *SPIE Optics + Photonics*. SPIE, pp. 14.
- Hufkens, K., Keenan, T.F., Flanagan, L.B., Scott, R.L., Bernacchi, C.J., Joo, E., Brunzell, N.A., Verfaillie, J., Richardson, A.D., 2016. Productivity of North American grasslands is increased under future climate scenarios despite rising aridity. *Nat. Clim. Chang.* 6, 710.
- Jiang, C., Ryu, Y., 2016. Multi-scale evaluation of global gross primary productivity and evapotranspiration products derived from breathing earth system simulator (BESS). *Remote Sens. Environ.* 186, 528–547.
- Jung, M., Reichstein, M., Schwalm, C.R., Huntingford, C., Sitch, S., Ahlstrom, A., Arneth, A., Camps-Valls, G., Ciais, P., Friedlingstein, P., Gans, F., Ichii, K., Jain, A.K., Kato, E., Papale, D., Poulter, B., Raduly, B., Rodenbeck, C., Tramonantana, G., Viovy, N., Wang, Y.P., Weber, U., Zaehle, S., Zeng, N., 2017. Compensatory water effects link yearly global land CO<sub>2</sub> sink changes to temperature. *Nature* 541, 516–520.
- Keenan, T.F., Riley, W.J., 2018. Greening of the land surface in the world's cold regions consistent with recent warming. *Nat. Clim. Chang.* 8, 825–828.
- Keenan, T.F., Gray, J., Friedl, M.A., Toomey, M., Bohrer, G., Hollinger, D.Y., Munger, J.W., O'Keefe, J., Schmid, H.P., SueWing, L., Yang, B., Richardson, A.D., 2014. Net carbon uptake has increased through warming-induced changes in temperate forest phenology. *Nat. Clim. Chang.* 4, 598–604.
- Larsen, K., 2015. *GAM: The Predictive Modeling Silver Bullet*. Multithreaded. Stitch Fix, pp. 30.
- Lim, P.O., Kim, H.J., Nam, H.G., 2007. Leaf senescence. *Annu. Rev. Plant Biol.* 58, 115–136.
- Liu, Q., Fu, Y.H., Zeng, Z., Huang, M., Li, X., Piao, S., 2016a. Temperature, precipitation, and insolation effects on autumn vegetation phenology in temperate China. *Glob. Chang. Biol.* 22, 644–655.
- Liu, Q., Fu, Y.H., Zhu, Z., Liu, Y., Liu, Z., Huang, M., Janssens, I.A., Piao, S., 2016b. Delayed autumn phenology in the northern hemisphere is related to change in both climate and spring phenology. *Glob. Chang. Biol.* 22, 3702–3711.
- Liu, D., Li, Y., Wang, T., Peylin, P., MacBean, N., Ciais, P., Jia, G.S., Ma, M.G., Ma, Y.M., Shen, M.G., Zhang, X.Z., Piao, S.L., 2018. Contrasting responses of grassland water and carbon exchanges to climate change between Tibetan Plateau and Inner Mongolia. *Agricultural and Forest Meteorology* 249, 163–175.
- Maseyk, K.S., Lin, T., Rotenberg, E., Grünzweig, J.M., Schwartz, A., Yakir, D., 2010. Physiology-phenology interactions in a productive semi-arid pine forest. *New Phytol.* 178, 603–616.
- Misra, G., Buras, A., Heurich, M., Asam, S., Menzel, A., 2018. LiDAR derived topography and forest stand characteristics largely explain the spatial variability observed in MODIS land surface phenology. *Remote Sens. Environ.* 218, 231–244.
- Park, T., Chen, C., Macias-Fauria, M., Tommervik, H., Choi, S., Winkler, A., Bhatt, U.S., Walker, D.A., Piao, S., Brovkin, V., Nemani, R.R., Myneni, R.B., 2019. Changes in timing of seasonal peak photosynthetic activity in northern ecosystems. *Glob. Chang. Biol.* 0.
- Peng, S., Piao, S., Ciais, P., Myneni, R.B., Chen, A., Chevallier, F., Dolman, A.J., Janssens, I.A., Penuelas, J., Zhang, G., Vicca, S., Wan, S., Wang, S., Zeng, H., 2013. Asymmetric effects of daytime and night-time warming on Northern Hemisphere vegetation. *Nature* 501, 88–92.
- Piao, S., Nan, H., Huntingford, C., Ciais, P., Friedlingstein, P., Sitch, S., Peng, S., Ahlstrom, A., Canadell, J.G., Cong, N., Levis, S., Levy, P.E., Liu, L., Lomas, M.R., Mao, J., Myneni, R.B., Peylin, P., Poulter, B., Shi, X., Yin, G., Viovy, N., Wang, T., Wang, X., Zaehle, S., Zeng, N., Zeng, Z., Chen, A., 2014. Evidence for a weakening relationship between interannual temperature variability and northern vegetation activity. *Nat. Commun.* 5, 5018.
- Piao, S.L., Liu, Z., Wang, T., Peng, S.S., Ciais, P., Huang, M.T., Ahlstrom, A., Burkhardt, J.F., Chevallier, F., Janssens, I.A., Jeong, S.J., Lin, X., Mao, J.F., Miller, J., Mohammad, A., Myneni, R.B., Penuelas, J., Shi, X.Y., Stohl, A., Yao, Y.T., Zhu, Z.C., Tans, P.P., 2017. Weakening temperature control on the interannual variations of spring carbon uptake across northern lands. *Nat. Clim. Chang.* 7, 359.
- Poulter, B., Frank, D., Ciais, P., Myneni, R.B., Andela, N., Bi, J., Broquet, G., Canadell, J.G., Chevallier, F., Liu, Y.Y., Running, S.W., Sitch, S., van der Werf, G.R., 2014. Contribution of semi-arid ecosystems to interannual variability of the global carbon cycle. *Nature* 509, 600–603.
- Reich, P.B., Walters, M.B., Ellsworth, D.S., 1992. Leaf life-span in relation to leaf, plant, and stand characteristics among diverse ecosystems. *Ecol. Monogr.* 62, 365–392.
- Richardson, A.D., Black, T.A., Ciais, P., Delbart, N., Friedl, M.A., Gobron, N., Hollinger, D.Y., Kutsch, W.L., Longdoz, B., Luysaert, S., Migliavacca, M., Montagnani, L., Munger, J.W., Moors, E., Piao, S., Rebmann, C., Reichstein, M., Saigusa, N., Tomelleri, E., Vargas, R., Varlagin, A., 2010. Influence of spring and autumn phenological transitions on forest ecosystem productivity. *Philos. Trans. R. Soc. Lond. Ser. B Biol. Sci.* 365, 3227–3246.
- Richardson, A.D., Keenan, T.F., Migliavacca, M., Ryu, Y., Sonnentag, O., Toomey, M., 2013. Climate change, phenology, and phenological control of vegetation feedbacks to the climate system. *Agric. For. Meteorol.* 169, 156–173.
- Ryu, Y., Baldocchi, D.D., Kobayashi, H., van Ingen, C., Li, J., Black, T.A., Beringer, J., van Gorsel, E., Knohl, A., Law, B.E., Rouspard, O., 2011. Integration of MODIS land and atmosphere products with a coupled-process model to estimate gross primary productivity and evapotranspiration from 1 km to global scales. *Glob. Biogeochem. Cycles* 25.
- Ryu, Y., Berry, J.A., Baldocchi, D.D., 2019. What is global photosynthesis? History, uncertainties and opportunities. *Remote Sens. Environ.* 223, 95–114.
- Schimel, D.S., 2010. Drylands in the earth system. *Science* 327, 418–419.
- Shang, R., Liu, R.G., Xu, M.Z., Liu, Y., Zuo, L., Ge, Q.S., 2017. The relationship between threshold-based and inflexion-based approaches for extraction of land surface phenology. *Remote Sens. Environ.* 199, 167–170.
- Shen, M., Tang, Y., Desai, A.R., Gough, C., Chen, J., 2014a. Can EVI-derived land-surface phenology be used as a surrogate for phenology of canopy photosynthesis? *Int. J. Remote Sens.* 35, 1162–1174.
- Shen, M., Zhang, G., Cong, N., Wang, S., Kong, W., Piao, S., 2014b. Increasing altitudinal gradient of spring vegetation phenology during the last decade on the Qinghai-Tibetan plateau. *Agric. For. Meteorol.* 189–190, 71–80.
- Shen, M., Piao, S., Cong, N., Zhang, G., Janssens, I.A., 2015a. Precipitation impacts on vegetation spring phenology on the Tibetan Plateau. *Glob. Chang. Biol.* 21, 3647–3656.
- Shen, M.G., Piao, S.L., Dorji, T., Liu, Q., Cong, N., Chen, X.Q., An, S., Wang, S.P., Wang, T., Zhang, G.X., 2015b. Plant phenological responses to climate change on the Tibetan plateau: research status and challenges. *Natl. Sci. Rev.* 2, 454–467.
- Shi, F.Z., Wu, X.C., Li, X.Y., Chen, D.L., Liu, H.Y., Liu, S.M., Hu, X., He, B., Shi, C.M., Wang, P., Mao, R., Ma, Y.J., Huang, Y.M., 2018. Weakening relationship between vegetation growth over the Tibetan plateau and large-scale climate variability. *Journal of Geophysical Research-Biogeosciences* 123, 1247–1259.
- Song, L., Guanter, L., Guan, K., You, L., Huete, A., Ju, W., Zhang, Y., 2018. Satellite sun-induced chlorophyll fluorescence detects early response of winter wheat to heat stress in the Indian Indo-Gangetic Plains. *Glob. Chang. Biol.* 24, 4023–4037.
- Wagle, P., Xiao, X.M., Torn, M.S., Cook, D.R., Matamala, R., Fischer, M.L., Jin, C., Dong, J.W., Biradar, C., 2014. Sensitivity of vegetation indices and gross primary production of tallgrass prairie to severe drought. *Remote Sens. Environ.* 152, 1–14.
- Wang, L., Tian, F., Wang, Y., Wu, Z., Schurgers, G., Fensholt, R., 2018a. Acceleration of global vegetation Greenup from combined effects of climate change and human land management. *Glob. Chang. Biol.* 24, 5484–5499.
- Wang, T., Liu, D., Piao, S., Wang, Y., Wang, X., Guo, H., Lian, X., Burkhardt, J.F., Ciais, P., Huang, M., Janssens, I., Li, Y., Liu, Y., Penuelas, J., Peng, S., Yang, H., Yao, Y., Yin, Y., Zhao, Y., 2018b. Emerging negative impact of warming on summer carbon uptake in northern ecosystems. *Nat. Commun.* 9, 5391.
- Wang, X.Y., Wu, C.Y., Peng, D.L., Gonsamo, A., Liu, Z.J., 2018c. Snow cover phenology affects alpine vegetation growth dynamics on the Tibetan plateau: satellite observed evidence, impacts of different biomes, and climate drivers. *Agric. For. Meteorol.* 256, 61–74.
- Wang, X., Xiao, J., Li, X., Cheng, G., Ma, M., Zhu, G., Altaf Arain, M., Andrew Black, T., Jassal, R.S., 2019. No trends in spring and autumn phenology during the global warming hiatus. *Nat. Commun.* 10, 2389.
- Wolf, S., Keenan, T.F., Fisher, J.B., Baldocchi, D.D., Desai, A.R., Richardson, A.D., Scott, R.L., Law, B.E., Litvak, M.E., Brunzell, N.A., Peters, W., van der Laan-Luijkx, I.T., 2016. Warm spring reduced carbon cycle impact of the 2012 US summer drought. *Proc. Natl. Acad. Sci. U. S. A.* 113, 5880–5885.
- Wu, C.Y., Chen, J.M., Black, T.A., Price, D.T., Kurz, W.A., Desai, A.R., Gonsamo, A., Jassal, R.S., Gough, C.M., Bohrer, G., Dragoni, D., Herbst, M., Gielen, B., Berninger, F., Vesala, T., Mammarella, I., Pilegaard, K., Blanken, P.D., 2013. Interannual variability of net ecosystem productivity in forests is explained by carbon flux phenology in autumn. *Glob. Ecol. Biogeogr.* 22, 994–1006.
- Wu, J., Guan, K., Hayek, M., Restrepo-Coupe, N., Wiedemann, K.T., Xu, X., Wehr, R., Christoffersen, B.O., Miao, G., da Silva, R., de Araujo, A.C., Oliveira, R.C., Camargo, P.B., Monson, R.K., Huete, A.R., Saleska, S.R., 2017. Partitioning controls on Amazon forest photosynthesis between environmental and biotic factors at hourly to interannual timescales. *Glob. Chang. Biol.* 23, 1240–1257.
- Wu, C.Y., Wang, X.Y., Wang, H.J., Ciais, P., Penuelas, J., Myneni, R.B., Desai, A.R., Gough, C.M., Gonsamo, A., Black, A.T., Jassal, R.S., Ju, W.M., Yuan, W.P., Fu, Y.S., Shen, M.G., Li, S.H., Liu, R.G., Chen, J.M., Ge, Q.S., 2018. Contrasting responses of autumn-leaf senescence to daytime and night-time warming. *Nat. Clim. Chang.* 8, 1092.
- Xia, J., Niu, S., Ciais, P., Janssens, I.A., Chen, J., Ammann, C., Arain, A., Blanken, P.D., Cescatti, A., Bonal, D., Buchmann, N., Curtis, P.S., Chen, S., Dong, J., Flanagan, L.B., Frankenberg, C., Georgiadis, T., Gough, C.M., Hui, D., Kiely, G., Li, J., Lund, M., Magliulo, V., Marcolla, B., Merbold, L., Montagnani, L., Moors, E.J., Olesen, J.E., Piao, S., Raschi, A., Rouspard, O., Suyker, A.E., Urbaniak, M., Vaccari, F.P., Varlagin, A., Vesala, T., Wilkinson, M., Weng, E., Wohlfahrt, G., Yan, L., Luo, Y., 2015. Joint control of terrestrial gross primary productivity by plant phenology and physiology. *Proc. Natl. Acad. Sci. U. S. A.* 112, 2788–2793.
- Xiao, X.M., Hollinger, D., Aber, J., Goltz, M., Davidson, E.A., Zhang, Q.Y., Moore, B., 2004a. Satellite-based modeling of gross primary production in an evergreen needleleaf forest. *Remote Sens. Environ.* 89, 519–534.
- Xiao, X.M., Zhang, Q.Y., Braswell, B., Urbanski, S., Boles, S., Wofsy, S., Berrien, M., Ojima, D., 2004b. Modeling gross primary production of temperate deciduous broadleaf forest using satellite images and climate data. *Remote Sens. Environ.* 91, 256–270.
- Xu, C., Liu, H., Williams, A.P., Yin, Y., Wu, X., 2016. Trends toward an earlier peak of the

- growing season in Northern Hemisphere mid-latitudes. *Glob. Chang. Biol.* 22, 2852–2860.
- Xu, X.Y., Riley, W.J., Koven, C.D., Jia, G.S., 2018. Observed and simulated sensitivities of spring Greenup to preseason climate in northern temperate and boreal regions. *Journal of Geophysical Research-Biogeosciences* 123, 60–78.
- Yang, K., He, J., Tang, W.J., Qin, J., Cheng, C.C.K., 2010. On downward shortwave and longwave radiations over high altitude regions: observation and modeling in the Tibetan plateau. *Agric. For. Meteorol.* 150, 38–46.
- Yu, G.R., Zhang, L.M., Sun, X.M., Fu, Y.L., Wen, X.F., Wang, Q.F., Li, S.G., Ren, C.Y., Song, X., Liu, Y.F., Han, S.J., Yan, J.H., 2008. Environmental controls over carbon exchange of three forest ecosystems in eastern China. *Glob. Chang. Biol.* 14, 2555–2571.
- Yu, G.R., Zhu, X.J., Fu, Y.L., He, H.L., Wang, Q.F., Wen, X.F., Li, X.R., Zhang, L.M., Zhang, L., Su, W., Li, S.G., Sun, X.M., Zhang, Y.P., Zhang, J.H., Yan, J.H., Wang, H.M., Zhou, G.S., Jia, B.R., Xiang, W.H., Li, Y.N., Zhao, L., Wang, Y.F., Shi, P.L., Chen, S.P., Xin, X.P., Zhao, F.H., Wang, Y.Y., Tong, C.L., 2013. Spatial patterns and climate drivers of carbon fluxes in terrestrial ecosystems of China. *Glob. Chang. Biol.* 19, 798–810.
- Zeng, Z.Z., Piao, S.L., Li, L.Z.X., Zhou, L.M., Ciais, P., Wang, T., Li, Y., Lian, X., Wood, E.F., Friedlingstein, P., Mao, J.F., Estes, L.D., Myneni, R.B., Peng, S.S., Shi, X.Y., Seneviratne, S.I., Wang, Y.P., 2017. Climate mitigation from vegetation biophysical feedbacks during the past three decades. *Nat. Clim. Chang.* 7, 432.
- Zhang, X., Friedl, M.A., Schaaf, C.B., Strahler, A.H., Hodges, J.C.F., Gao, F., Reed, B.C., Huete, A., 2003. Monitoring vegetation phenology using MODIS. *Remote Sens. Environ.* 84, 471–475.
- Zhang, Y., Xiao, X.M., Jin, C., Dong, J.W., Zhou, S., Wagle, P., Joiner, J., Guanter, L., Zhang, Y.G., Zhang, G.L., Qin, Y.W., Wang, J., Moore, B., 2016a. Consistency between sun-induced chlorophyll fluorescence and gross primary production of vegetation in North America. *Remote Sens. Environ.* 183, 154–169.
- Zhang, Y., Xiao, X.M., Zhou, S., Ciais, P., McCarthy, H., Luo, Y.Q., 2016b. Canopy and physiological controls of GPP during drought and heat wave. *Geophys. Res. Lett.* 43, 3325–3333.
- Zhang, Y., Xiao, X., Wu, X., Zhou, S., Zhang, G., Qin, Y., Dong, J., 2017. A global moderate resolution dataset of gross primary production of vegetation for 2000–2016. *Sci Data* 4, 170165.
- Zhou, Y.Z., Jia, G.S., 2016. Precipitation as a control of vegetation phenology for temperate steppes in China. *Atmospheric and Oceanic Science Letters* 9, 162–168.
- Zhou, S., Zhang, Y., Caylor, K.K., Luo, Y.Q., Xiao, X.M., Ciais, P., Huang, Y.F., Wang, G.Q., 2016. Explaining inter-annual variability of gross primary productivity from plant phenology and physiology. *Agric. For. Meteorol.* 226, 246–256.
- Zhou, S., Zhang, Y., Ciais, P., Xiao, X., Luo, Y., Caylor, K.K., Huang, Y., Wang, G., 2017. Dominant role of plant physiology in trend and variability of gross primary productivity in North America. *Sci. Rep.* 7, 41366.
- Zu, J.X., Zhang, Y.J., Huang, K., Liu, Y.J., Chen, N., Cong, N., 2018. Biological and climate factors co-regulated spatial-temporal dynamics of vegetation autumn phenology on the Tibetan plateau. *Int. J. Appl. Earth Obs. Geoinf.* 69, 198–205.